ONE-DIMENSIONAL FERRONEMATICS IN A CHANNEL: ORDER RECONSTRUCTION, BIFURCATIONS AND MULTISTABILITY*

JAMES DALBY†, PATRICK E. FARRELL‡, APALA MAJUMDAR§, AND JINGMIN XIA‡

Abstract. We study a model system with nematic and magnetic orders, within a channel geometry modelled by an interval, $[-D, D]$. The system is characterised by a tensor-valued nematic order parameter $\mathbf{Q}$ and a vector-valued magnetisation $\mathbf{M}$, and the observable states are modelled as stable critical points of an appropriately defined free energy. In particular, the full energy includes a nemato-magnetic coupling term characterised by a parameter c. We (i) derive L^∞ bounds for $\mathbf{Q}$ and $\mathbf{M}$; (ii) prove a uniqueness result in parameter regimes defined by c, D and material- and temperature-dependent correlation lengths; (iii) analyse order reconstruction solutions, possessing domain walls, and their stabilities as a function of D and c and (iv) perform numerical studies that elucidate the interplay of c and D for multistability.

Key words. ferronematics, bifurcation analysis, stability, liquid crystals

AMS subject classifications. 34D20, 34C23, 76A15

1. Introduction.

Nematic liquid crystals (NLCs) are classical examples of mesophases that combine fluidity with long-range orientational order [12]. Molecules in NLCs tend to align, on average, along certain locally preferred directions, referred to as *directors*. NLCs are anisotropic materials with a direction-dependent response to light and external fields, and are thus used in a range of electro-optical devices, e.g., the multi-billion dollar liquid crystal display industry [17]. Moreover, NLCs typically rely on their dielectric anisotropy, i.e., directional response to external electric fields, for applications. Their responses to external magnetic fields are much weaker (perhaps seven orders of magnitude smaller) than their dielectric response [25] and consequently, nemato-magnetic coupling has been poorly exploited for NLC applications, e.g., sensors, displays, microfluidics etc.

In the pioneering work of [6], Brochard and de Gennes suggested that a suspension of magnetic nanoparticles (MNPs) in a NLC host could induce a spontaneous magnetisation without any external magnetic fields, and substantially enhance nemato-magnetic material response. This new class of materials with nematic and magnetic orders is referred to as *ferronematics*, with notable theoretical contributions by [8, 9] and experimental realisations by [24], later by [22] where the crucial factors for the stability of ferronematic suspensions are identified. Ferronematics have tremendous potential, both theoretically and in applications as magnetic-nematic materials for meta-materials, bio-materials, topological materials, and nano-systems, to name a

*Submitted to the editors DATE.

Funding: PEF is supported by the Engineering and Physical Sciences Research Council [grant numbers EP/R029423/1 and EP/V001493/1]. AM and JD are supported by a DST-UKIERI grant on "Theoretical and experimental studies of suspensions of magnetic nanoparticles, their applications and generalizations", a Leverhulme International Academic Fellowship, the University of Strathclyde's New Professor Fund and an OCIAM Visiting Fellowship. AM thanks Giacomo Canevari for informative discussions on Γ-convergence and Neela Nataraj,Ruma Maity for discussions on asymptotic analysis in the $l \to 0$ limit. AM thanks Varsha Banerjee and Konark Bisht for their collaboration in 2019. JX is supported by the EPSRC Centre for Doctoral Training in Partial Differential Equations [grant number EP/L015811/1] and the National University of Defense Technology.

†Department of Mathematics, University of Strathclyde, UK (james.dalby@strath.ac.uk).

‡Mathematical Institute, University of Oxford, UK (patrick.farrell@maths.ox.ac.uk, jingmin.xia@maths.ox.ac.uk).

§Department of Mathematics, University of Strathclyde, UK (apala.majumdar@strath.ac.uk).

few [19].

In this work, we study a dilute suspension of MNPs in a NLC-filled channel, $\tilde{\Omega} = [-L, L] \times [-D, D] \times [0, G]$, where $L \gg D$, L is the length of the channel, D is the channel width and G is the channel height. In other words, we assume a uniform distribution of MNPs (much smaller than the physical domain dimensions) such that the average distance between the MNPs is much larger than the MNP size, and the total volume fraction of MNPs is small. These MNPs generate a spontaneous magnetisation even without any external magnetic fields, by means of the NLC-MNP interactions. Thus, the system has two order parameters: (i) a nematic tensor parameter $\mathbf{Q}$ with two degrees of freedom, that contains information about the director corresponding to the preferred direction of molecular alignment and (ii) a magnetisation vector $\mathbf{M}$ generated by the suspended MNPs.

Following the methods in [4] and [9], we model the physically observable $(\mathbf{Q}, \mathbf{M})$-profiles as minimisers of an appropriately defined ferronematic free energy, which includes a nemato-magnetic coupling energy characterised by a coupling parameter $c > 0$. This coupling energy favours co-alignment between the nematic director and $\mathbf{M}$ (one can define other forms of the coupling energy that do not favour such co-alignment). Furthermore, the microscopic details of the MNP properties (shape, size, anchoring, volume fraction etc.) and the NLC-MNP interactions are homogenised in the dilute limit, to yield the nemato-magnetic coupling energy. Under various modelling assumptions, as described in the next section, energy minimisers exist and are given by solutions of the corresponding boundary value problem for $\mathbf{Q}$ and $\mathbf{M}$, on an interval $[-D, D]$, where D is the physical length scale. In addition, we prescribe conflicting Dirichlet conditions for $\mathbf{Q}$ and $\mathbf{M}$, although the physically relevant choices of the boundary conditions for $\mathbf{M}$ are unclear. We expect our qualitative conclusions to be unchanged for Neumann boundary conditions for $\mathbf{M}$.

The pure nematic case, i.e., when $c = 0$, is well-understood; see for example [11, 18]. We therefore first study how the solution landscapes for $c = 0$ are perturbed by the nemato-magnetic coupling energy, in the dilute limit. Our first notable analysis concerns the *vacuum manifold* for the minimisers of a spatially homogeneous problem or equivalently, the minimisers of the bulk potential characterised by two dimensionless parameters, (ξ, c). For dilute ferronematics, ξ is small, i.e., the magnetisation effects are weaker than the nematic effects and we set $\xi = 1$ throughout this manuscript, unless otherwise stated. We illustrate later how c perturbs the well-studied uncoupled vacuum manifold as a linear perturbation for small c. Our second non-trivial result concerns a maximum principle argument (Theorem 2.5) for the critical points of the ferronematic free energy, and we obtain an L^∞ bound for the critical points $(\mathbf{Q}, \mathbf{M})$ in terms of c. This bound reduces to the L^∞ bound for the uncoupled problems when $c = 0$. Third, in Theorem 2.7 we prove that the ferronematic energy has a unique critical point, and hence minimiser, for $D \ll c_1 \frac{\xi_n}{\sqrt{c_0^2 + c^2}}$, where ξ_n is the nematic correlation length, c_0 is a computable constant and c_1 is a constant independent of all model parameters.

With these crucial analytic ingredients at hand, we can partially address questions related to how the solution landscapes for $c = 0$ are perturbed by $c > 0$ in this paper. In the pure nematic case ($c = 0$), the model problem admits a unique order reconstruction (OR) solution for $D \ll c_2 \xi_n$, for some positive constant c_2 (in fact, $c_2 = c_1/c_0$) independent of model parameters [18]. In the ferronematic case, an OR solution exists for all D (Theorem 3.1), with distinct domain walls (defined by $\mathbf{Q} = 0$ and $\mathbf{M} = 0$) that separate distinctly ordered polydomains. Essentially, the

polydomains have a constant non-zero $(\mathbf{Q},\mathbf{M})$-profile and the profile jumps across a domain wall, which represents the surface discontinuity in the three dimensional channel setting. Moreover, OR solutions are globally stable for $D \ll c_1 \frac{\xi_n}{\sqrt{c_0^2+c^2}}$ and thus c shrinks their domain of stability. In Theorem 3.4, as D increases, we show that OR solutions become unstable by means of a Γ-convergence argument and second variation analysis. This is further corroborated by numerical experiments and computations of bifurcation diagrams, for two specific values of c. Increasing D, we find that the magnetic profiles are tailored by the nematic profiles in the channel interior, as would be expected in a dilute ferronematic with dominant nematic effects.

The nemato-magnetic coupling introduces additional possibilities for the interplay between nematic and magnetic domain walls (absent when $c = 0$), new defect structures, and novel bifurcations accompanied by novel solution branches for large D. We do not address these questions fully in this manuscript but present a large number of examples that will support and guide future studies on these lines.

The paper is organised as follows. In the next section, we describe the ferronematic model and give some qualitative results of interest, e.g., existence, uniqueness, homogeneous solutions etc. We then consider the order reconstruction model in section 3, where similar qualitative results and the stability of OR solutions are presented. Furthermore, we provide numerical results in section 4 to verify our theoretical analysis. Finally, some conclusions and perspectives are summarised in section 5.

2. Model Problem. We consider a dilute ferronematic suspension sandwiched inside the three dimensional channel $\tilde{\Omega}$ with strong anchoring on the xz-planes and free boundary conditions on the yz- and xy-planes. From a modelling perspective, we assume that the structural profile is invariant across the height of the channel, and along the length of the channel, since $L \gg D$, with no boundary constraints imposed at the ends $x = \pm L$. Hence, we restrict ourselves to a one-dimensional channel geometry: $\Omega = [-D, D]$ in what follows. As noted from section 1, the ferronematic suspension is described by two order parameters: a symmetric, traceless 2×2 matrix $\mathbf{Q}$, i.e., $\mathbf{Q} \in S_0 \coloneqq \{\mathbf{Q} \in \mathbb{M}^{2\times 2} : Q_{ij} = Q_{ji}, Q_{ii} = 0\}$, and a two-dimensional vector, $\mathbf{M} = (M_1, M_2)$. Here, $\mathbb{M}^{2\times 2}$ denotes all 2×2 matrices. The nematic order parameter $\mathbf{Q}$ can be written as

$$\mathbf{Q} = s(2\mathbf{n} \otimes \mathbf{n} - \mathbf{I}), \tag{2.1}$$

where s is a scalar order parameter, and $\mathbf{n}$ is the nematic director (a unit-vector describing the direction of orientational ordering in the xy-plane) and $\mathbf{I}$ is the 2×2 identity matrix. Moreover, s can be interpreted as a measure of the degree of the orientational order for $\mathbf{n}$, so that the nodal sets of s (i.e., where $s = 0$) define nematic defects in the xy-plane. We denote the two independent components of $\mathbf{Q}$ by Q_{11} and Q_{12} such that

$$Q_{11} = s\cos 2\vartheta, \quad Q_{12} = s\sin 2\vartheta,$$

when $\mathbf{n} = (\cos\vartheta, \sin\vartheta)$ and ϑ denotes the angle between $\mathbf{n}$ and the horizontal axis. To avoid writing $\mathbf{Q}$ in the matrix form $\left[\begin{smallmatrix} Q_{11} & Q_{12} \\ Q_{12} & -Q_{11} \end{smallmatrix}\right]$, we henceforth label $\mathbf{Q}$ in terms of its two independent components (Q_{11}, Q_{12}), when this causes no confusions. We therefore define the vector norm, $|\mathbf{Q}| = \sqrt{Q_{11}^2 + Q_{12}^2}$, as opposed to a matrix norm. Similarly, we define $|\mathbf{M}| = \sqrt{M_1^2 + M_2^2}$.

Following the methods in [22, 4], the ferronematic free energy is given by the sum of three energies for low temperatures: a Landau–de Gennes type nematic energy of $\mathbf{Q}$,

a magnetisation energy of $\mathbf{M}$ and a coupling energy between $\mathbf{Q}$ and $\mathbf{M}$. This coupling energy can be viewed as the homogenised version of a Rapini–Papoular type surface anchoring energy on the MNP surfaces that dictates the co-alignment between $\mathbf{n}$ and $\mathbf{M}$ [10], in the dilute limit of ferronematic suspensions. We adopt the rescalings as in [4], so to use the rescaled domain $\Omega = [-1, 1]$, and the total rescaled and dimensionless ferronematic free energy is

$$\begin{aligned} F(Q_{11}, Q_{12}, M_1, M_2) \coloneqq \int_\Omega \Bigg\{ & \frac{l_1}{2}\left[\left(\frac{\mathrm{d}Q_{11}}{\mathrm{d}y}\right)^2 + \left(\frac{\mathrm{d}Q_{12}}{\mathrm{d}y}\right)^2\right] + \left(Q_{11}^2 + Q_{12}^2 - 1\right)^2 \\ & + \frac{\xi l_2}{2}\left[\left(\frac{\mathrm{d}M_1}{\mathrm{d}y}\right)^2 + \left(\frac{\mathrm{d}M_2}{\mathrm{d}y}\right)^2\right] + \frac{\xi}{4}\left(M_1^2 + M_2^2 - 1\right)^2 \\ & - cQ_{11}\left(M_1^2 - M_2^2\right) - 2cQ_{12}M_1M_2 \Bigg\} \,\mathrm{d}y. \end{aligned} \tag{2.2}$$

Here, $l_1 > 0$ and $l_2 > 0$ are scaled elastic constants (inversely proportional to D, i.e., the physical channel width), $\xi > 0$ is a parameter that weighs the relative strength of the nematic and magnetic energies and c is a coupling parameter. For dilute ferronematic suspensions, the MNP interactions are "small" and the NLC-MNP interactions are absorbed by the coupling energy, thus the magnetic energy is not the dominant energetic contribution and $\xi \leq 1$ [9]. Substituting (2.1) into the coupling energy, we observe that

$$-cQ_{11}\left(M_1^2 - M_2^2\right) - 2cQ_{12}M_1M_2 \propto -c\left(\mathbf{n}\cdot\mathbf{M}\right)^2.$$

We only focus on positive coupling, i.e., $c > 0$ in this work so that this coupling energy favours co-alignment between the nematic director $\mathbf{n}$ and magnetic vector $\mathbf{M}$, i.e., $\mathbf{n}\cdot\mathbf{M} = \pm 1$.

Regarding boundary conditions, we work with Dirichlet conditions for $\mathbf{Q}$ and $\mathbf{M}$ on the boundaries $y = \pm 1$ i.e.

$$Q_{11}(-1) = M_1(-1) = 1, \tag{2.3a}$$

$$Q_{12}(-1) = Q_{12}(1) = M_2(-1) = M_2(1) = 0, \tag{2.3b}$$

$$Q_{11}(1) = M_1(1) = -1. \tag{2.3c}$$

Here, the boundary conditions for $\mathbf{Q}$ correspond to $\mathbf{n} = (1, 0)$ on $y = -1$ and $\mathbf{n} = (0, 1)$ on $y = 1$, hence, we have planar boundary conditions on $y = -1$ and normal/homeotropic boundary conditions on $y = +1$. Furthermore, the boundary conditions for $\mathbf{M}$ describe a π-rotation between the bounding plates, $y = \pm 1$.

The admissible space is given by

$$\begin{aligned} \mathcal{A} = \big\{ & \mathbf{Q} \in W^{1,2}\left(\Omega; S_0\right), \mathbf{M} \in W^{1,2}\left(\Omega; \mathbb{R}^2\right), \\ & \mathbf{Q} \text{ and } \mathbf{M} \text{ satisfy the boundary conditions (2.3)} \big\}. \end{aligned} \tag{2.4}$$

The Sobolev space $W^{1,2}$ is the space of all square-integrable $(\mathbf{Q}, \mathbf{M})$ with square-integrable first weak derivatives, which is a standard choice for such variational problems. The stable, physically relevant and potentially observable $(\mathbf{Q}, \mathbf{M})$-profiles are local or global energy minimisers of the full energy (2.2) subject to the boundary conditions in (2.3), in $\mathcal{A}$. They are in fact, classical solutions of the associated Euler–Lagrange equations [4]

$$l_1 \frac{\mathrm{d}^2 Q_{11}}{\mathrm{d}y^2} = 4Q_{11}(Q_{11}^2 + Q_{12}^2 - 1) - c\left(M_1^2 - M_2^2\right), \tag{2.5a}$$

$$l_1\frac{\mathrm{d}^2Q_{12}}{\mathrm{d}y^2}=4Q_{12}(Q_{11}^2+Q_{12}^2-1)-2cM_1M_2, \tag{2.5b}$$

$$\xi l_2\frac{\mathrm{d}^2M_1}{\mathrm{d}y^2}=\xi M_1\left(M_1^2+M_2^2-1\right)-2cQ_{11}M_1-2cQ_{12}M_2, \tag{2.5c}$$

$$\xi l_2\frac{\mathrm{d}^2M_2}{\mathrm{d}y^2}=\xi M_2\left(M_1^2+M_2^2-1\right)+2cQ_{11}M_2-2cQ_{12}M_1, \tag{2.5d}$$

The first result concerns a brief proof of the existence of a global minimiser of the free energy (2.2), in $\mathcal{A}$.

THEOREM 2.1. *For all positive values of (l_1,l_2,c,ξ), there exists at least one minimiser $(Q_{11}^*,Q_{12}^*,M_1^*,M_2^*)$ of the ferronematic free energy (2.2) in the admissible space (2.4). Moreover, this minimiser is a (classical) solution of the Euler–Lagrange equations (2.5a)-(2.5d) subject to the boundary conditions (2.3).*

Remark 2.2. For brevity of notations, we omit $(\Omega;S_0)$ and $(\Omega;\mathbb{R}^2)$ in the Sobolev spaces hereafter, whenever it causes no confusions.

Proof. The admissible space (2.4) is nonempty as $(Q_{11},Q_{12},M_1,M_2)=(-y,0,-y,0)$ belongs to $\mathcal{A}$ and it satisfies the boundary conditions (2.3). The ferronematic energy (2.2) is quadratic and thus, convex in the gradient of all four state variables (Q_{11},Q_{12},M_1,M_2) and hence, lower semicontinuous [13]. Furthermore, the coupling energy can be decomposed as follows

$$\begin{aligned}-cQ_{11}\left(M_1^2-M_2^2\right)-2cQ_{12}M_1M_2&\geq -c(M_1^2+M_2^2)(Q_{11}+Q_{12})\\&\geq -\frac{c}{2}\left(\epsilon\left(Q_{11}+Q_{12}\right)^2+\frac{1}{\epsilon}\left(M_1^2+M_2^2\right)^2\right)\\&\geq -\frac{c}{2}\left(2\epsilon\left(Q_{11}^2+Q_{12}^2\right)+\frac{1}{\epsilon}\left(M_1^2+M_2^2\right)^2\right),\end{aligned}$$

where $\epsilon>0$ is arbitrary. Hence, the energy density is bounded from below as

$$\begin{aligned}&\frac{l_1}{2}\left[\left(\frac{\mathrm{d}Q_{11}}{\mathrm{d}y}\right)^2+\left(\frac{\mathrm{d}Q_{12}}{\mathrm{d}y}\right)^2\right]+\left(Q_{11}^2+Q_{12}^2-1\right)^2+\frac{\xi l_2}{2}\left[\left(\frac{\mathrm{d}M_1}{\mathrm{d}y}\right)^2+\left(\frac{\mathrm{d}M_2}{\mathrm{d}y}\right)^2\right]\\&\quad+\frac{\xi}{4}\left(M_1^2+M_2^2-1\right)^2-cQ_{11}\left(M_1^2-M_2^2\right)-2cQ_{12}M_1M_2\\&\geq\frac{l_1}{2}\left[\left(\frac{\mathrm{d}Q_{11}}{\mathrm{d}y}\right)^2+\left(\frac{\mathrm{d}Q_{12}}{\mathrm{d}y}\right)^2\right]+\frac{\xi l_2}{2}\left[\left(\frac{\mathrm{d}M_1}{\mathrm{d}y}\right)^2+\left(\frac{\mathrm{d}M_2}{\mathrm{d}y}\right)^2\right]\\&\quad+\left[Q_{11}^2+Q_{12}^2-\left(1+\frac{c\epsilon}{2}\right)\right]^2+\left(\frac{\xi\epsilon-2c}{4\epsilon}\right)\left(M_1^2+M_2^2-\frac{\epsilon\xi}{\xi\epsilon-2c}\right)^2\\&\quad-\left(c\epsilon+\frac{c^2\epsilon^2}{4}+\frac{c\xi}{2(\xi\epsilon-2c)}\right),\end{aligned}$$

and thus the full energy (2.2) is coercive provided $\epsilon>\frac{2c}{\xi}$. The existence of a minimiser in the admissible space $\mathcal{A}$ therefore follows by the direct method in the calculus of variations [13]. We can follow the arguments from elliptic regularity in [3] and [21] to deduce that the minimiser is a classical solution of (2.5a)-(2.5d). ∎

2.1. Homogeneous solutions and asymptotics as $c\to 0$ and $c\to\infty$. The critical points of the bulk energy density $f(Q_{11},Q_{12},M_1,M_2)$, particularly the bulk

energy minimisers for different values of (c, ξ), are crucial for the analysis of the full variational problem in (2.5a)-(2.5d). We denote the bulk energy density in (2.2) by

$$f(Q_{11}, Q_{12}, M_1, M_2) \coloneqq \left(Q_{11}^2 + Q_{12}^2 - 1\right)^2 + \frac{\xi}{4}\left(M_1^2 + M_2^2 - 1\right)^2 - cQ_{11}\left(M_1^2 - M_2^2\right) - 2cQ_{12}M_1M_2. \tag{2.6}$$

Using the substitutions

$$\begin{aligned} Q_{11} &= \rho\cos(\theta), Q_{12} = \rho\sin(\theta), \\ M_1 &= \sigma\cos(\phi), M_2 = \sigma\sin(\phi), \end{aligned} \tag{2.7}$$

the bulk energy density becomes

$$f(\rho, \sigma, \theta, \phi) = (\rho^2 - 1)^2 + \frac{\xi}{4}(\sigma^2 - 1)^2 - c\rho\sigma^2\cos(2\phi - \theta). \tag{2.8}$$

The critical points $(\rho(c, \xi), \sigma(c, \xi))$, $\rho, \sigma \geq 0$ are solutions of the following system of algebraic equations:

$$4\rho\cos(\theta)\left(\rho^2 - 1\right) - c\sigma^2\cos(2\phi) = 0, \tag{2.9a}$$

$$4\rho\sin(\theta)\left(\rho^2 - 1\right) - c\sigma^2\sin(2\phi) = 0, \tag{2.9b}$$

$$\xi\sigma\cos(\phi)\left(\sigma^2 - 1\right) - 2\sigma\rho c\cos(\theta - \phi) = 0, \tag{2.9c}$$

$$\xi\sigma\sin(\phi)\left(\sigma^2 - 1\right) - 2\sigma\rho c\sin(\theta - \phi) = 0. \tag{2.9d}$$

There are two trivial solutions, i.e., $\rho = \sigma = 0$; $\rho = 1$ and $\sigma = 0$, which exist for all real-valued c and ξ. For these trivial solutions, θ and ϕ are undetermined. For ferronematic solutions, we need $\rho, \sigma \neq 0$ in order to capture the nemato-magnetic coupling. The equations (2.9) can be explicitly solved; firstly, (2.9c) and (2.9d) give

$$\sigma^2 = 1 + \frac{2\rho c\cos(\theta - \phi)}{\xi\cos(\phi)} \text{ and } \sigma^2 = 1 + \frac{2\rho c\sin(\theta - \phi)}{\xi\sin(\phi)},$$

respectively, which in turn require that

$$\frac{\cos(\theta - \phi)}{\cos(\phi)} = \frac{\sin(\theta - \phi)}{\sin(\phi)} \implies 2\phi - \theta = n\pi \quad \text{for } n \in \mathbb{Z},$$

imposing constraints on the relative alignment of $\mathbf{n}$ and $\mathbf{M}$. Furthermore, multiplying (2.9a) by $\sin(\theta)$, (2.9b) by $\cos(\theta)$, following similar steps for (2.9c) and (2.9d), and using the constraint $2\phi = \theta + n\pi$, we obtain

$$\rho^3 - \rho\left(1 + \frac{c^2}{2\xi}\right) - \frac{c}{4} = 0, \tag{2.10a}$$

$$\rho^3 - \rho\left(1 + \frac{c^2}{2\xi}\right) + \frac{c}{4} = 0. \tag{2.10b}$$

Here, (2.10a) corresponds to $2\phi - \theta = 2n\pi$ whereas (2.10b) corresponds to $2\phi - \theta = (2n + 1)\pi$, i.e., an odd multiple of π. Once ρ is determined by (2.10), σ is given by

$$\sigma^2 = 1 + \frac{2\rho c}{\xi}, \tag{2.11a}$$

$$\sigma^2 = 1 - \frac{2\rho c}{\xi}; \tag{2.11b}$$

where (2.11a) (resp. (2.11b)) is associated with (2.10a) (resp. (2.10b)).

To solve (2.10a), let $\rho = S+T$ and recall that $(S+T)^3 - 3ST(S+T) - (S^3+T^3) = 0$, then we have

$$ST = \frac{1}{3}\left(1 + \frac{c^2}{2\xi}\right), \qquad S^3 + T^3 = \frac{c}{4},$$

from which we deduce that S^3 and T^3 are roots of the quadratic equation

$$z^2 - \frac{c}{4}z + \frac{1}{27}\left(1 + \frac{c^2}{2\xi}\right)^3 = 0,$$

i.e., $z_\pm = \frac{c}{8} \pm \sqrt{\frac{c^2}{64} - \frac{1}{27}\left(1 + \frac{c^2}{2\xi}\right)^3}$. Hence, S and T are given by

$$S = \omega_j \left(\frac{c}{8} + \sqrt{\frac{c^2}{64} - \frac{1}{27}\left(1 + \frac{c^2}{2\xi}\right)^3}\right)^{\frac{1}{3}} =: \omega_j \Theta_1, \tag{2.12a}$$

$$T = \omega_k \left(\frac{c}{8} - \sqrt{\frac{c^2}{64} - \frac{1}{27}\left(1 + \frac{c^2}{2\xi}\right)^3}\right)^{\frac{1}{3}} =: \omega_k \Theta_2, \tag{2.12b}$$

for $j, k \in \{1, 2, 3\}$, where $\omega_1 = 1, \omega_2 = \frac{-1+\sqrt{3}\mathrm{i}}{2}$ and $\omega_3 = \frac{-1-\sqrt{3}\mathrm{i}}{2}$ are the cube roots of unity. Throughout this work, we use the notation $\mathrm{i} = \sqrt{-1}$. This yields nine possible roots of (2.10a), of which only three are viable choices since $ST = \frac{1}{3}\left(1 + \frac{c^2}{2\xi}\right)$ and thus, $\omega_j\omega_k = 1$. Therefore, the viable roots of (2.10a) are given by, for $k \in \{1, 2, 3\}$,

$$\rho = \omega_k \Theta_1 + \omega_k^2 \Theta_2, \tag{2.13}$$

and the corresponding values of σ are

$$\sigma = \sqrt{1 + \frac{2c}{\xi}\left(\omega_k \Theta_1 + \omega_k^2 \Theta_2\right)} \tag{2.14}$$

with $2\phi - \theta$ being an even multiple of π.

The cubic equation (2.10b) can be tackled similarly so that the relevant roots of (2.10b) and the corresponding values of σ are given by

$$\begin{aligned}\rho &= \omega_k \left(-\frac{c}{8} + \sqrt{\frac{c^2}{64} - \frac{1}{27}\left(1 + \frac{c^2}{2\xi}\right)^3}\right)^{\frac{1}{3}} + \omega_k^2 \left(-\frac{c}{8} - \sqrt{\frac{c^2}{64} - \frac{1}{27}\left(1 + \frac{c^2}{2\xi}\right)^3}\right)^{\frac{1}{3}} \\ &=: \omega_k \Lambda_1 + \omega_k^2 \Lambda_2,\end{aligned} \tag{2.15}$$

and

$$\sigma = \sqrt{1 - \frac{2c}{\xi}\left(\omega_k \Lambda_1 + \omega_k^2 \Lambda_2\right)}, \tag{2.16}$$

with $2\phi - \theta$ being an odd multiple of π, for $k \in \{1, 2, 3\}$. Hence, the solution pairs $(\rho(c, \xi), \sigma(c, \xi))$ for the algebraic system (2.9) are given by ((2.13),(2.14)) and ((2.15),(2.16)).

Amongst the admissible critical points, we require ρ and σ to be non-negative and real-valued. In fact, if $27c^2 \leq 64\left(1 + \frac{c^2}{2\xi}\right)$ then both (2.13) and (2.15) yield a real-valued ρ for each $k \in \{1, 2, 3\}$ (one can check this with De Moivre's formula), whilst for $27c^2 > 64\left(1 + \frac{c^2}{2\xi}\right)$, (2.13) and (2.15) have a real solution only if $k = 1$. Furthermore, if ρ is real, (2.14) gives a real-valued σ when $-\frac{2c}{\xi}\rho \leq 1$, whilst (2.16) yields real-valued σ if $\frac{2c}{\xi}\rho \leq 1$. Regarding non-negative solution pairs, we simply enumerate the solution pairs with $\rho \geq 0$ and choose the positive root for σ.

For simplicity, we now focus on the special case of $\xi = 1$. The inequality $27c^2 < 64\left(1 + \frac{c^2}{2}\right)^3$ holds for all $c \geq 0$, and hence, both (2.13) and (2.15) yield real-valued ρ. Therefore, we have the following positive real solutions:

$$\rho = \Theta_1 + \Theta_2, \tag{2.17a}$$

$$\rho = \Lambda_1 + \Lambda_2, \tag{2.17b}$$

$$\rho = \omega_3\Lambda_1 + \omega_2\Lambda_2, \tag{2.17c}$$

and the corresponding values of σ are

$$\sigma = \sqrt{1 + 2c\,(\Theta_1 + \Theta_2)}, \tag{2.18a}$$

$$\sigma = \sqrt{1 - 2c\,(\Lambda_1 + \Lambda_2)}, \tag{2.18b}$$

$$\sigma = \sqrt{1 - 2c\,(\omega_3\Lambda_1 + \omega_2\Lambda_2)}. \tag{2.18c}$$

Moreover, the solutions in (2.18a) and (2.18c) correspond to a real-valued σ for all $c > 0$, while (2.18b) is real for $c \leq \frac{1}{2}$. Henceforth, we do not consider the solution pair ((2.17b),(2.18b)) in this manuscript.

The next task is to determine which solution pair, (ρ, σ), minimises the bulk energy density (2.8), for $c \geq 0$ with $\xi = 1$. It is enough to observe that $f(0, 0) = \frac{5}{4}$ and $f(1, 0) = \frac{1}{4}$, and identify which of the non-trivial solution pairs, if any, satisfy $f(\rho, \sigma) < \frac{1}{4}$. In Figure 1, we plot the bulk energy density (2.8) as a function of c for each non-trivial solution pair ((2.17a), (2.18a)), ((2.17c), (2.18c)) and observe that ((2.17a),(2.18a)) is the global energy minimiser for all positive values of c.

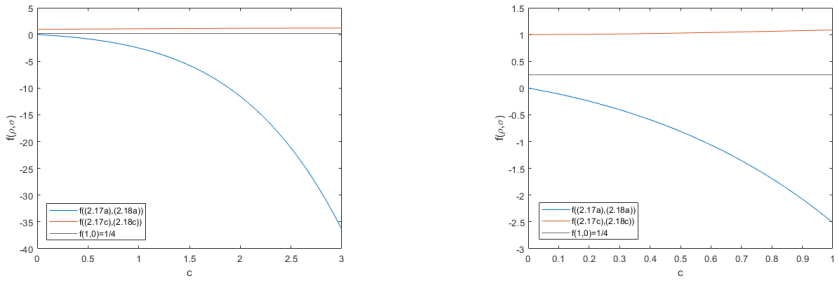

Fig. 1: Plots of the bulk energy density (2.8) at $(\rho, \sigma) =$ ((2.17a),(2.18a)) and ((2.17c),(2.18c)) as functions of c with $\xi = 1$ for (left) $c \in [0, 3]$ and (right) $c \in [0, 1]$.

Next, we compute asymptotic expansions for the minimising pair ((2.17a), (2.18a)) as $c \to 0$, $c \to \infty$ respectively. As $c \to 0$, we expect the minimising pair to approach $(\rho, \sigma) \to (1, 1)$, since $(\rho, \sigma) = (1, 1)$ is the minimiser of the bulk energy density with $c = 0$. To this end, we first approximate the square root terms in (2.17a) as

$$\sqrt{-\frac{c^2}{64} + \frac{1}{27}\left(1 + \frac{c^2}{2}\right)^3} \approx \frac{1}{3\sqrt{3}}\left(1 + \frac{69c^2}{128}\right),$$

by applying the binomial formula. Then using De Moivre's formula and an appropriate binomial formula, the first cube root is approximated by

$$\begin{aligned}\Theta_1 = \left(\frac{c}{8} + \sqrt{\frac{c^2}{64} - \frac{1}{27}\left(1 + \frac{c^2}{2}\right)^3}\right)^{\frac{1}{3}} &\approx \left(\frac{\mathrm{i}}{3\sqrt{3}}\right)^{\frac{1}{3}}\left(1 + \left(\frac{3\sqrt{3}c}{8\mathrm{i}} + \frac{69c^2}{128}\right)\right)^{\frac{1}{3}} \\ &= \left(\frac{1}{2} + \frac{\sqrt{3}\mathrm{i}}{6}\right)\left(1 + \frac{\sqrt{3}c}{8\mathrm{i}} + \frac{29c^2}{128} + \mathcal{O}(c^3)\right) \\ &\approx \frac{1}{2} + \frac{c}{16} + \mathrm{i}P(c).\end{aligned}$$

In the last approximation, we have ignored $\mathcal{O}(c^2)$ terms for small c and $P(c) := \frac{\sqrt{3}}{6} - \frac{\sqrt{3}c}{16}$. The second cube root is the complex conjugate of the first cube root in (2.17a), and thus for the solution pair ((2.17a), (2.18a)), we have as $c \to 0$ that

$$\rho \approx 1 + \frac{c}{8}, \tag{2.19a}$$

$$\sigma^2 \approx 1 + 2c + \frac{c^2}{4}.. \tag{2.19b}$$

For large $c \gg 1$, the square root in (2.17a) is given by (to leading order),

$$\sqrt{\frac{1}{27}\left(1 + \frac{c^2}{2}\right)^3 - \frac{c^2}{64}} \approx \frac{\sqrt{6}c^3}{36}. \tag{2.20}$$

Similarly, the first cube root in (2.17a) can be approximated to leading order as

$$\Theta_1 \approx \left(\frac{c}{8} + \mathrm{i}\frac{\sqrt{6}c^3}{36}\right)^{\frac{1}{3}} \approx \left(\frac{\sqrt{3} + \mathrm{i}}{2}\right)\left(\frac{\sqrt{6}}{36}\right)^{\frac{1}{3}} c.$$

Applying similar arguments to the second cube root, we deduce that for $c \gg 1$

$$\rho \approx \left(\frac{\sqrt{2}}{4}\right)^{\frac{1}{3}} c, \tag{2.21a}$$

$$\sigma^2 \approx 1 + \sqrt{2}c^2. \tag{2.21b}$$

Hence, both ρ and σ grow linearly with c for large $c \gg 1$, for the bulk energy minimiser ((2.17a), (2.18a)).

Remark 2.3. For the uncoupled problem with $c = 0$, we have nine solution pairs (ρ, σ) (with θ, ϕ undetermined) of the system (2.9), namely,

$$(0, 0),\ (0, \pm 1),\ (\pm 1, 0),\ (\pm 1, \pm 1), \tag{2.22}$$

where all sign combinations are possible. In the limit $c \to 0$, we expect each of the solution pairs ((2.13), (2.14)) and ((2.15), (2.16)) to reduce to a solution of the uncoupled problem. In fact, ((2.13), (2.14)) and ((2.15), (2.16)) recover all of the solution pairs in (2.22), except $(0,0)$ and $(\pm 1, 0)$. However, these unrecovered solution pairs, $(\rho, \sigma) = \{(0,0), (\pm 1, 0)\}$ are solutions of the system (2.9) for arbitrary $c \geq 0$, and thus not perturbed for $c > 0$.

2.2. Maximum principle and uniqueness results. We now return to the full problem (2.5a)-(2.5d) subject to the boundary conditions (2.3), which necessarily has inhomogeneous non-constant solutions. We first derive a non-trivial maximum principle argument for the solutions of (2.5a)-(2.5d), followed by a uniqueness result in a certain asymptotic regime (i.e., $l \to \infty$).

Remark 2.4. For simplicity and brevity, we take $l_1 = l_2 = l$ and $\xi = 1$ hereafter. The cases of $l_1 \neq l_2$ and $\xi \neq 1$ can be tackled using similar mathematical methods, although ξ is necessarily small for dilute ferronematic suspensions.

THEOREM 2.5. *(Maximum principle) There exists an L^∞ bound for the solutions, $(Q_{11}, Q_{12}, M_1, M_2)$ of the system (2.5a)-(2.5d) subject to the boundary conditions (2.3). Specifically,*

$$Q_{11}^2(y) + Q_{12}^2(y) \leq (\rho^*)^2, \;\; M_1^2(y) + M_2^2(y) \leq 1 + 2c\rho^* \quad \forall y \in [-1, 1], \tag{2.23}$$

where ρ^* is given by

$$\rho^* = \left(\frac{c}{8} + \sqrt{\frac{c^2}{64} - \frac{1}{27}\left(1 + \frac{c^2}{2}\right)^3} \right)^{\frac{1}{3}} + \left(\frac{c}{8} - \sqrt{\frac{c^2}{64} - \frac{1}{27}\left(1 + \frac{c^2}{2}\right)^3} \right)^{\frac{1}{3}}. \tag{2.24}$$

Proof. Assume that, $|\mathbf{Q}| = \sqrt{Q_{11}^2 + Q_{12}^2}$, and, $|\mathbf{M}| = \sqrt{M_1^2 + M_2^2}$, attain their maxima at two distinct points $y_1, y_2 \in (-1, 1)$, respectively, then we have

$$\frac{\mathrm{d}^2}{\mathrm{d}y^2}\left(\frac{1}{2}|\mathbf{Q}|^2\right)(y_1) \leq 0 \text{ and } \frac{\mathrm{d}^2}{\mathrm{d}y^2}\left(\frac{1}{2}|\mathbf{M}|^2\right)(y_2) \leq 0.$$

Multiplying (2.5a) by Q_{11}, (2.5b) by Q_{12}, adding the resulting equations, and using the identity $\frac{\mathrm{d}^2}{\mathrm{d}y^2}\left(\frac{1}{2}|\mathbf{Q}|^2\right) = \frac{\mathrm{d}^2 Q_{11}}{\mathrm{d}y^2} Q_{11} + \frac{\mathrm{d}^2 Q_{12}}{\mathrm{d}y^2} Q_{12} + \left(\frac{\mathrm{d}Q_{11}}{\mathrm{d}y}\right)^2 + \left(\frac{\mathrm{d}Q_{12}}{\mathrm{d}y}\right)^2$, we obtain the necessary condition

$$\left[4\left(Q_{11}^2 + Q_{12}^2\right)\left(Q_{11}^2 + Q_{12}^2 - 1\right) - c\left(Q_{11}(M_1^2 - M_2^2) + 2Q_{12}M_1M_2\right)\right]\Big|_{y=y_1} \leq 0. \tag{2.25}$$

Similarly, multiplying (2.5c) by M_1, (2.5d) by M_2, adding the resulting equations, and using the identity $\frac{\mathrm{d}^2}{\mathrm{d}y^2}\left(\frac{1}{2}|\mathbf{M}|^2\right) = \frac{\mathrm{d}^2 M_1}{\mathrm{d}y^2} M_1 + \frac{\mathrm{d}^2 M_2}{\mathrm{d}y^2} M_2 + \left|\frac{\mathrm{d}\mathbf{M}}{\mathrm{d}y}\right|^2$, the following necessary inequality must hold:

$$\left[\left(M_1^2 + M_2^2\right)\left(M_1^2 + M_2^2 - 1\right) - 2c\left(Q_{11}(M_1^2 - M_2^2) + 2Q_{12}M_1M_2\right)\right]\Big|_{y=y_2} \leq 0. \tag{2.26}$$

Substituting (2.7) with $\rho = |\mathbf{Q}| \geq 0$ and $\sigma = |\mathbf{M}| \geq 0$ into (2.25) and (2.26), we obtain

$$0 \geq \left[4\rho^2(\rho^2 - 1) - c\rho\sigma^2\cos(\theta - 2\phi)\right]\Big|_{y=y_1} \geq \left[4\rho^2(\rho^2 - 1) - c\rho\sigma^2\right]\Big|_{y=y_1},$$

$$\implies \left(\rho^3-\rho-\frac{c\sigma^2}{4}\right)\Big|_{y=y_1}\leq 0, \tag{2.27}$$

and

$$0\geq \left[\sigma^2(\sigma^2-1)-2c\rho\sigma^2\cos(\theta-2\phi)\right]\Big|_{y=y_2}\geq \left[\sigma^2(\sigma^2-1)-2c\rho\sigma^2\right]\Big|_{y=y_2},$$
$$\implies \left(\sigma^2-1-2c\rho\right)\Big|_{y=y_2}\leq 0,$$

respectively. We then immediately deduce that $\sigma^2(y)\leq 1+2c\rho(y_2)$ for all $y\in[-1,1]$, as $|\mathbf{M}|$ attains its maximum at y_2, and since $\rho(y_1)\geq\rho(y_2)$ (as $|\mathbf{Q}|$ attains its maximum at y_1), we further have $\sigma^2(y)\leq 1+2c\rho(y_1)$ for arbitrary $y\in[-1,1]$, particularly at $y=y_1$. Using this in (2.27), we have

$$0\geq\left(\rho^3-\rho-\frac{c\sigma^2}{4}\right)\Big|_{y=y_1}\geq\left(\rho^3-\rho\left(1+\frac{c^2}{2}\right)-\frac{c}{4}\right)\Big|_{y=y_1},$$

which holds provided that ρ is less than or equal to the largest positive root of the cubic polynomial $\rho^3-\rho\left(1+\frac{c^2}{2}\right)-\frac{c}{4}$. From the discussions in subsection 2.1, its largest positive root is given by (2.17a) and thus $\rho(y_1)\leq\rho^*$. The L^∞ bounds for ρ and σ are an immediate consequence, i.e.,

$$\rho(y)\leq\rho^*,\ \sigma^2(y)\leq 1+2c\rho^*\quad\forall y\in[-1,1].$$

Note that if $y_1=y_2$, the proof follows similarly since $\rho(y_1)=\rho(y_2)$. ∎

Remark 2.6. For $c=0$, the upper bounds (2.23) reduce to $Q_{11}^2+Q_{12}^2\leq 1$, $M_1^2+M_2^2\leq 1$, which are the Ginzburg–Landau bounds in [20] for $\mathbf{Q}$ and $\mathbf{M}$. Moreover, if c is small, we use the derivations of (2.19a) and (2.19b) to deduce the following approximated L^∞ bounds,

$$Q_{11}^2+Q_{12}^2\leq 1+\frac{c}{4},\ M_1^2+M_2^2\leq 1+2c,$$

to leading order in c. Hence, the nemato-magnetic coupling perturbs the Ginzburg–Landau bounds linearly, for small values of the coupling parameter c.

With the L^∞ bounds at hand, one can prove that there is a unique critical point of (2.2), which is necessarily the global energy minimiser, in the $l\to\infty$ limit.

THEOREM 2.7. *(Uniqueness of minimisers for sufficiently large l) For a fixed c and for l sufficiently large, there exists a unique critical point (and hence global minimiser) of the full energy (2.2), in the admissible space (2.4).*

Proof. We first show that the free energy (2.2) is strictly convex using the maximum principle. In fact, we let $(\mathbf{Q},\mathbf{M}),(\overline{\mathbf{Q}},\overline{\mathbf{M}})\in\mathcal{A}$ so that $(\mathbf{Q}-\overline{\mathbf{Q}})\in W_0^{1,2}$ and $(\mathbf{M}-\overline{\mathbf{M}})\in W_0^{1,2}$, where $W_0^{1,2}$ is the closure of C_0^∞ with respect to the $W^{1,2}$-norm. Note that

$$F\left(\frac{\mathbf{Q}+\overline{\mathbf{Q}}}{2},\frac{\mathbf{M}+\overline{\mathbf{M}}}{2}\right)=\frac{1}{2}\left[F(\mathbf{Q},\mathbf{M})+F(\overline{\mathbf{Q}},\overline{\mathbf{M}})\right]+\int_\Omega\Bigg\{f\left(\frac{\mathbf{Q}+\overline{\mathbf{Q}}}{2},\frac{\mathbf{M}+\overline{\mathbf{M}}}{2}\right)$$
$$-\frac{1}{2}\left[f(\mathbf{Q},\mathbf{M})+f(\overline{\mathbf{Q}},\overline{\mathbf{M}})\right]-\frac{l}{8}\left[\left(\frac{\mathrm{d}\mathbf{Q}}{\mathrm{d}y}\right)-\left(\frac{\mathrm{d}\overline{\mathbf{Q}}}{\mathrm{d}y}\right)\right]^2$$

$$
\begin{aligned}
&- \frac{l}{8}\left[\left(\frac{\mathrm{d}\mathbf{M}}{\mathrm{d}y}\right) - \left(\frac{\mathrm{d}\overline{\mathbf{M}}}{\mathrm{d}y}\right)\right]^2\Bigg\}\,\mathrm{d}y \\
\leq &\frac{1}{2}\left[F\left(\mathbf{Q},\mathbf{M}\right) + F\left(\overline{\mathbf{Q}},\overline{\mathbf{M}}\right)\right] + \int_\Omega \Bigg\{ f\left(\frac{\mathbf{Q}+\overline{\mathbf{Q}}}{2}, \frac{\mathbf{M}+\overline{\mathbf{M}}}{2}\right) \\
&- \frac{1}{2}\left[f\left(\mathbf{Q},\mathbf{M}\right) + f\left(\overline{\mathbf{Q}},\overline{\mathbf{M}}\right)\right]\Bigg\}\,\mathrm{d}y - \frac{l}{16}\|\mathbf{Q}-\overline{\mathbf{Q}}\|_{L^2}^2 \\
&- \frac{l}{16}\|\mathbf{M}-\overline{\mathbf{M}}\|_{L^2}^2,
\end{aligned} \tag{2.28}
$$

where f is the bulk energy density (2.6) with $\xi = 1$, and we have used the Poincaré inequality with the Poincaré constant $c_p = \frac{1}{2}$ in the last inequality. We estimate the second partial derivatives of f, using the L^∞ bounds above, yielding

$$
\begin{aligned}
&\frac{\partial^2 f}{\partial Q_{1i}\partial Q_{1j}} = 4\delta_{ij}\left(Q_{11}^2 + Q_{12}^2 - 1\right) + 8Q_{1i}Q_{1j} \leq 4\left(3(\rho^*)^2 - 1\right) =: a_1, \\
&\left|\frac{\partial^2 f}{\partial M_i \partial M_j}\right| \leq B(5c\rho^* + 1) =: a_2, \\
&\left|\frac{\partial^2 f}{\partial Q_{1i}\partial M_j}\right| \leq Ac\sqrt{1+2c\rho*} =: a_3,
\end{aligned}
$$

for $i, j \in \{1, 2\}$, where δ_{ij} is the Kronecker delta symbol and A, B are constants independent of c, for $\xi = 1$. Using methods parallel to [18, Lemma 8.2], we have

$$
\begin{aligned}
&\int_\Omega \left\{ f\left(\frac{\mathbf{Q}+\overline{\mathbf{Q}}}{2}, \frac{\mathbf{M}+\overline{\mathbf{M}}}{2}\right) - \frac{1}{2}\left[f\left(\mathbf{Q},\mathbf{M}\right) + f\left(\overline{\mathbf{Q}},\overline{\mathbf{M}}\right)\right]\right\}\mathrm{d}y \\
&\qquad \leq a_1\|\mathbf{Q}-\overline{\mathbf{Q}}\|_{L^2}^2 + a_2\|\mathbf{M}-\overline{\mathbf{M}}\|_{L^2}^2 + a_3\|\mathbf{Q}-\overline{\mathbf{Q}}\|_{L^2}\|\mathbf{M}-\overline{\mathbf{M}}\|_{L^2}.
\end{aligned} \tag{2.29}
$$

Note that

$$
\left\|\mathbf{Q}-\overline{\mathbf{Q}}\right\|_{L^2}\left\|\mathbf{M}-\overline{\mathbf{M}}\right\|_{L^2} \leq \frac{1}{2}\left(\epsilon\left\|\mathbf{Q}-\overline{\mathbf{Q}}\right\|_{L^2}^2 + \epsilon^{-1}\left\|\mathbf{M}-\overline{\mathbf{M}}\right\|_{L^2}^2\right) \quad \forall \epsilon > 0.
$$

We take $\epsilon = 2$ for convenience and then substitute (2.29) into (2.28), and thus

$$
\begin{aligned}
F\left(\frac{\mathbf{Q}+\overline{\mathbf{Q}}}{2}, \frac{\mathbf{M}+\overline{\mathbf{M}}}{2}\right) \leq &\frac{1}{2}\left[F\left(\mathbf{Q},\mathbf{M}\right) + F\left(\overline{\mathbf{Q}},\overline{\mathbf{M}}\right)\right] + \left(a_1 + a_3 - \frac{l}{16}\right)\|\mathbf{Q}-\overline{\mathbf{Q}}\|_{L^2}^2 \\
&+ \left(a_2 + \frac{a_3}{4} - \frac{l}{16}\right)\|\mathbf{M}-\overline{\mathbf{M}}\|_{L^2}^2.
\end{aligned}
$$

Hence, for $l > l^*(c) = \max\{16(a_1+a_3), 4(4a_2+a_3)\}$, it holds that

$$
F\left(\frac{\mathbf{Q}+\overline{\mathbf{Q}}}{2}, \frac{\mathbf{M}+\overline{\mathbf{M}}}{2}\right) < \frac{1}{2}F\left(\mathbf{Q},\mathbf{M}\right) + \frac{1}{2}F\left(\overline{\mathbf{Q}},\overline{\mathbf{M}}\right)
$$

for all $\mathbf{Q}, \overline{\mathbf{Q}} \in W^{1,2}$ and $\mathbf{M}, \overline{\mathbf{M}} \in W^{1,2}$ such that $\mathbf{Q} \neq \overline{\mathbf{Q}}$, $\mathbf{M} \neq \overline{\mathbf{M}}$. Therefore, F is strictly convex.

Now assume that for $l \in (l^*, \infty)$, there exist two solutions $(\mathbf{Q}, \mathbf{M})$ and $\left(\overline{\mathbf{Q}}, \overline{\mathbf{M}}\right)$ of (2.5a)-(2.5d) in the admissible space $\mathcal{A}$. Then the mapping

$$
[0,1] \ni t \mapsto F\left(t\mathbf{Q} + (1-t)\overline{\mathbf{Q}}, t\mathbf{M} + (1-t)\overline{\mathbf{M}}\right)
$$

is C^1 (continuously differentiable) and its derivative vanishes at $t = 0, 1$. However, this contradicts the strict convexity of F and hence, the uniqueness result follows. ∎

Remark 2.8. Recalling the definitions of the dimensionless parameters in [4]:

$$l_1 = \frac{L}{D^2|A|},\ l_2 = \frac{\kappa}{D^2|\alpha|},\ c = \frac{\gamma\mu_0}{|A|}\sqrt{\frac{C}{2|A|}}\frac{|\alpha|}{\beta}. \tag{2.30}$$

From Theorem 2.7, the conditions $l = l_1 = l_2 > l^*(c) = \max\{16(a_1+a_3), 4(4a_2+a_3)\}$ guarantee the uniqueness of a solution for the system (2.5a)-(2.5d). The parameters a_1, a_2, a_3 grow as c^2 for large c, thus $l^*(c)$ is also an increasing function of c. Therefore, the condition $l > l^*(c)$ is equivalent to $\frac{c_1^2 L}{D^2|A|(c_0^2+c^2)} \gg 1$ for some constants c_0, c_1 or $D \ll \sqrt{\frac{c_1^2 L}{|A|(c_0^2+c^2)}} =: c_1\frac{\xi_n}{\sqrt{c_0^2+c^2}}$, i.e., when the physical length D is much smaller than an enhanced material-dependent length scale $c_1\frac{\xi_n}{\sqrt{c_0^2+c^2}}$. For $c = 0$, we recover the uniqueness results reported in [18] and [11].

2.3. Convergence analysis for $l \to \infty$ and $l \to 0$. For a fixed $c > 0$, the $l \to \infty$ limit corresponds to very narrow channels with $D \ll \sqrt{\frac{L}{|A|(c_0^2+c^2)}}$ as discussed in Remark 2.8, for which the system (2.5a)-(2.5d) has a unique solution in the admissible space $\mathcal{A}$. From the maximum principle Theorem 2.5, $\|\mathbf{Q}\|_{L^\infty}$ and $\|\mathbf{M}\|_{L^\infty}$ are bounded independently of l, as shown in (2.23). Furthermore, in this limit, one can easily see that (2.5a)-(2.5d) reduce to the Laplace equations

$$\begin{aligned} \frac{\mathrm{d}^2 Q_{11}}{\mathrm{d}y^2} &= 0, \quad \frac{\mathrm{d}^2 Q_{12}}{\mathrm{d}y^2} = 0, \\ \frac{\mathrm{d}^2 M_1}{\mathrm{d}y^2} &= 0, \quad \frac{\mathrm{d}^2 M_2}{\mathrm{d}y^2} = 0, \end{aligned} \tag{2.31}$$

subject to (2.3), which admits the unique solution as shown below:

$$(\mathbf{Q}^\infty, \mathbf{M}^\infty) = (Q_{11}^\infty, Q_{12}^\infty, M_1^\infty, M_2^\infty) = (-y, 0, -y, 0). \tag{2.32}$$

In fact, (2.32) is an **order reconstruction** solution, as introduced in section 3, with linear profiles for Q_{11} and M_1. In the next theorem, we study the convergence of solutions $(\mathbf{Q}^l, \mathbf{M}^l)$ of (2.5a)-(2.5d) to $(\mathbf{Q}^\infty, \mathbf{M}^\infty)$ as $l \to \infty$, using the method of sub- and super-solutions as in [14].

THEOREM 2.9. *Assume $l > l^*$. Let $(\mathbf{Q}^l, \mathbf{M}^l)$ be the unique solution of the Euler–Lagrange equations (2.5a)-(2.5d) in the admissible space (2.4), subject to the boundary conditions (2.3). Then $(\mathbf{Q}^l, \mathbf{M}^l)$ converge to $(\mathbf{Q}^\infty, \mathbf{M}^\infty)$ as $l \to \infty$ with the following estimates:*

$$\forall j = 1, 2, \quad \|Q_{1j}^l - Q_{1j}^\infty\|_{L^\infty} \le \alpha_1 l^{-1},\ \|M_j^l - M_j^\infty\|_{L^\infty} \le \alpha_2 l^{-1}, \tag{2.33}$$

for positive constants α_1, α_2 independent of l.

Proof. Recalling [14, Proposition 3.1] and comparing equations (2.5a)-(2.5d) with the Laplace equations (2.31), we have for $j = 1, 2$,

$$-l^{-1}\left(4\rho^*\left((\rho^*)^2 - 1\right) + c\left(1 + 2c\rho^*\right)\right) \le \frac{\mathrm{d}^2}{\mathrm{d}y^2}\left(Q_{1j}^l - Q_{1j}^\infty\right) \tag{2.34a}$$

$$\leq l^{-1}\left(4\rho^*\left((\rho^*)^2-1\right)+c\,(1+2c\rho^*)\right) \quad \text{in } \Omega,$$

$$Q_{1j}^l - Q_{1j}^\infty = 0 \quad \text{on } \partial\Omega, \tag{2.34b}$$

(2.34c)

$$-l^{-1}6c\rho^*(1+2c\rho^*)^{\frac{1}{2}} \leq \frac{\mathrm{d}^2}{\mathrm{d}y^2}(M_j^l - M_j^\infty) \leq l^{-1}6c\rho^*(1+2c\rho^*)^{\frac{1}{2}} \quad \text{in } \Omega,$$

$$M_j^l - M_j^\infty = 0 \quad \text{on } \partial\Omega. \tag{2.34d}$$

Here, the L^∞ bound (2.23) from the maximum principle has been used in the inequalities above. Let $v_k \in C^\infty(\Omega;\mathbb{R})$, $k=1,2$, be solutions of

$$\begin{cases} \dfrac{\mathrm{d}^2 v_1}{\mathrm{d}y^2} = 4\rho^*\left((\rho^*)^2-1\right)+c\,(1+2c\rho^*) & \text{in } \Omega, \\ \dfrac{\mathrm{d}^2 v_2}{\mathrm{d}y^2} = 6c\rho^*\,(1+2c\rho^*)^{\frac{1}{2}} & \text{in } \Omega, \\ v_k = 0 \quad \text{for } k=1,2 & \text{on } \partial\Omega. \end{cases}$$

Then each v_k only depends on the coupling parameter c. Hence, by the classical sub- and super-solution method, $-l^{-1}v_1$ is a sub-solution and $l^{-1}v_1$ is a super-solution for the representative components of $(\mathbf{Q}^l - \mathbf{Q}^\infty)$, and similarly, $-l^{-1}v_2$ is a sub-solution and $l^{-1}v_2$ is a super-solution for each of the vector components of $(\mathbf{M}^l - \mathbf{M}^\infty)$. The estimates then follow and the proof is complete. ∎

In the $l \to \infty$ limit, we compute useful asymptotic expansions of the OR solution branch for large l and small c, by setting $l = \frac{1}{c}$ in the Euler–Lagrange equations (2.5a)-(2.5d) and expanding around $(\mathbf{Q}^\infty, \mathbf{M}^\infty)$ as shown below:

$$Q_{11}(y) = -y + cf_2(y) + c^2 f_3(y) + \mathcal{O}(c^3), \quad M_1 = -y + cf_2^*(y) + c^2 f_3^*(y) + \mathcal{O}(c^3).$$

Substituting the above into (2.5a) and (2.5d) (with $l = \frac{1}{c}$) and equating powers of c, we solve the computed second order ordinary differential equations for f_2, f_3, f_2^*, f_3^*, subject to the boundary conditions $f_2(-1) = f_2(1) = f_3(-1) = f_3(1) = 0$ and $f_2^*(-1) = f_2^*(1) = f_3^*(-1) = f_3^*(1) = 0$. This gives

$$Q_{11}(y) = -y + c\left(-\frac{1}{5}y^5 + \frac{2}{3}y^3 - \frac{7}{15}y\right) + c^2 p(y) + \mathcal{O}(c^3), \tag{2.35}$$

and

$$M_1(y) = -y + c\left(-\frac{1}{20}y^5 + \frac{1}{6}y^3 - \frac{7}{60}y\right) + c^2 q(y) + \mathcal{O}(c^3), \tag{2.36}$$

for $l = \frac{1}{c}$ and $l \gg 1$. Here,

$$p(y) = -\frac{1}{30}y^9 + \frac{22}{105}y^7 - \frac{31}{75}y^5 - \frac{1}{12}y^4 + \frac{14}{45}y^3 - \frac{233}{3150}y + \frac{1}{12},$$

and

$$q(y) = -\frac{1}{480}y^9 + \frac{11}{840}y^7 - \frac{31}{1200}y^5 - \frac{1}{6}y^4 + \frac{7}{360}y^3 - \frac{233}{50400}y + \frac{1}{6}.$$

We can further check the validity of these expansions, (2.35) and (2.36), numerically. To this end, we compare $(\cdot)^{num}$ and $(\cdot)^{asymp}$ in the L^∞-norm, where $(\cdot)^{num}$ is the numerical solution and $(\cdot)^{asymp}$ corresponds to the asymptotic expansion, depending on the truncation of the expansions in (2.35) and (2.36). For instance, a first order truncation yields

$$Q_{11}^{asymp} = -y + c\left(-\frac{1}{5}y^5 + \frac{2}{3}y^3 - \frac{7}{15}y\right),$$
$$M_1^{asymp} = -y + c\left(-\frac{1}{20}y^5 + \frac{1}{6}y^3 - \frac{7}{60}y\right).$$

The left hand column of Figure 2 shows a first order convergence by truncating the expansions up to $\mathcal{O}(c^0)$, whilst a first order truncation leads to a second order convergence as shown in the middle column of Figure 2 and finally, in the right hand column, a truncation up to $\mathcal{O}(c^2)$ demonstrates an almost third order convergence with respect to c, for both Q_{11} and M_1.

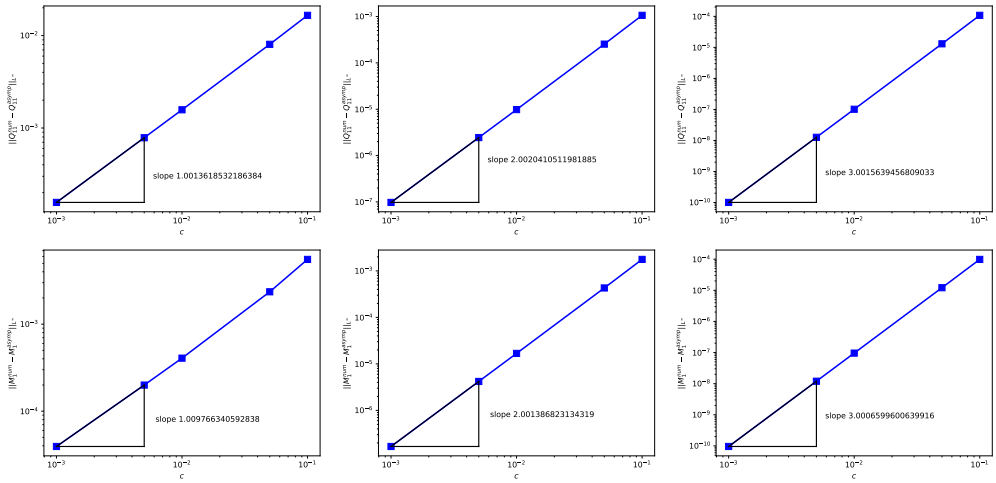

Fig. 2: Log-log plots of $\|Q_{11}^{num} - Q_{11}^{asymp}\|_{L^\infty}$ (top row) and $\|M_1^{num} - M_1^{asymp}\|_{L^\infty}$ (bottom row). Left: truncating asymptotic expansions (2.35) and (2.36) at c^0. Middle: truncating asymptotic expansions at c^1. Right: truncating asymptotic expansions at c^2.

Next, we study the convergence of solutions $(\mathbf{Q}^l, \mathbf{M}^l)$ in the $l \to 0$ limit, with c fixed. To this end, we rewrite the free energy (2.2) as

(2.37)
$$\frac{1}{l}F(Q_{11}, Q_{12}, M_1, M_2) \coloneqq \int_\Omega \left\{ \frac{1}{2}\left[\left(\frac{\mathrm{d}Q_{11}}{\mathrm{d}y}\right)^2 + \left(\frac{\mathrm{d}Q_{12}}{\mathrm{d}y}\right)^2\right] + \right.$$
$$\left. + \frac{1}{2}\left[\left(\frac{\mathrm{d}M_1}{\mathrm{d}y}\right)^2 + \left(\frac{\mathrm{d}M_2}{\mathrm{d}y}\right)^2\right] + \frac{1}{l}\bar{f}(Q_{11}, Q_{12}, M_1, M_2)\right\} \mathrm{d}y,$$

where

$$\bar{f}(Q_{11},Q_{12},M_1,M_2) \coloneqq \left(Q_{11}^2+Q_{12}^2-1\right)^2+\frac{1}{4}\left(M_1^2+M_2^2-1\right)^2 - cQ_{11}\left(M_1^2-M_2^2\right)-2cQ_{12}M_1M_2-\alpha(c)\geq 0 \tag{2.38}$$

and the c-dependent constant, $\alpha(c)$, is the minimum value of the bulk energy density.

Consider the following admissible test maps for sufficiently small l, with $Q_{12}^t(y)=M_2^t(y)\equiv 0$ for $y\in[-1,1]$ and

$$Q_{11}^t(y)=\begin{cases} g(y), & y\in\left[-1,-1+\sqrt{l}\right),\\ \rho^*, & y\in\left(-1+\sqrt{l},1-\sqrt{l}\right),\\ h(y), & y\in\left(1-\sqrt{l},1\right]. \end{cases}$$

Here, g linearly interpolates between ρ^* and $g(-1)=1$; h linearly interpolates between ρ^* and $h(1)=-1$. Similarly, we use the following test map for M_1:

$$M_1^t(y)=\begin{cases} g^*(y), & y\in\left[-1,-1+\sqrt{l}\right),\\ \sqrt{1+2c\rho^*}, & y\in\left(-1+\sqrt{l},1-\sqrt{l}\right),\\ h^*(y), & y\in\left(1-\sqrt{l},1\right]. \end{cases}$$

Here, g^* linearly interpolates between $\sqrt{1+2c\rho^*}$ and $g^*(-1)=1$; h^* linearly interpolates between $\sqrt{1+2c\rho^*}$ and $h^*(1)=-1$. Recall from subsection 2.1 that $\bar{f}\left(\rho^*,0,\sqrt{1+2c\rho^*},0\right)=0$. It is straightforward to check that

$$\frac{1}{l}F\left(Q_{11}^t,0,M_1^t,0\right)\leq\frac{C}{\sqrt{l}}$$

for a positive constant C independent of l, with l small enough. Hence, for an energy minimiser $(\mathbf{Q}^l,\mathbf{M}^l)$ of the full energy (2.2) with small l, we have the following energy bound

$$\frac{1}{l}F\left(Q_{11}^l,Q_{12}^l,M_1^l,M_2^l\right)\leq\frac{C}{\sqrt{l}},$$

and thus

$$\int_{-1}^{1}\bar{f}\left(Q_{11}^l,Q_{12}^l,M_1^l,M_2^l\right)\,\mathrm{d}y\leq C\sqrt{l}\to 0\quad\text{as } l\to 0.$$

Furthermore, since $\bar{f}\geq 0$ by its definition (2.38), we deduce that $\bar{f}\left(Q_{11}^l,Q_{12}^l,M_1^l,M_2^l\right)\equiv 0$ almost everywhere as $l\to 0$. Hence, we expect that as $l\to 0$, the energy minimisers, $\left(\mathbf{Q}^l,\mathbf{M}^l\right)$ converge almost everywhere to the minimisers of the modified bulk potential, $\bar{f}$ defined in (2.38). The minimisers of $\bar{f}$ belong to the set

$$\mathcal{A}_{\min}\coloneqq\left\{(Q_{11},Q_{12},M_1,M_2)=\left(\rho^*\cos 2\phi,\rho^*\sin 2\phi,\sqrt{1+2c\rho^*}\cos\phi,\sqrt{1+2c\rho^*}\sin\phi\right)\right\},$$

where ρ^* is given by (2.24) and ϕ is an arbitrary angle. The set $\mathcal{A}_{\min}$ is clearly a continuum. As $l\to 0$, we expect the energy minimisers to minimise the Dirichlet energy of $\mathbf{Q}$ and $\mathbf{M}$ in the constrained set $\mathcal{A}_{\min}$, so that the limiting minimisers in the $l\to 0$ limit are given by:

$$\mathbf{Q}^0(c,y)=\rho^*(\cos(2\phi_0(y)),\sin(2\phi_0(y))),\ \mathbf{M}^0(c,y)=\sqrt{1+2c\rho^*}\left(\cos(\phi_0(y)),\sin(\phi_0(y))\right). \tag{2.39}$$

where there are two choices of ϕ_0, dictated by the boundary conditions for $\mathbf{M}$:

$$\frac{\mathrm{d}^2\phi_0}{\mathrm{d}y^2} = 0, \tag{2.40a}$$

$$\phi_0(-1) = 0, \phi_0(1) = \pi \quad \text{or} \quad \phi_0(-1) = 0, \phi_0(1) = -\pi. \tag{2.40b}$$

In subsection 4.3, we numerically demonstrate that the energy minimisers, $\left(\mathbf{Q}^l, \mathbf{M}^l\right)$ indeed converge to one of the two limiting maps in $\mathcal{A}_{\min}$, defined above, almost everywhere except near $y = \pm 1$ (and interior points associated with jumps in $(2\phi_0 - \theta_0)$, since $2\phi_0 - \theta$ is constrained to be an even multiple of 2π, in the $l \to 0$ limit). There are necessarily boundary layers near $y = \pm 1$, since the limiting maps in $\mathcal{A}_{\min}$ do not satisfy the boundary conditions at $y = \pm 1$.

We do not prove convergence results in the $l \to 0$ limit rigorously in this paper, since this requires a delicate Γ-convergence analysis for a vector-valued problem with four degrees of freedom, and for which the bulk energy minimisers are not a finite discrete set, with additional complications from the choice of boundary conditions. Therefore, we feel that this warrants a separate study in its own right.

3. Order reconstruction solutions. The results in section 2 concern the full problem (2.5a)-(2.5d) or ferronematic solutions with four degrees of freedom, $(\mathbf{Q}, \mathbf{M}) = (Q_{11}, Q_{12}, M_1, M_2)$. It is evident from the Euler–Lagrange equations (2.5a)-(2.5d), that we always have a branch of solutions with $Q_{12} = M_2 = 0$. We refer to such solutions with only two degrees of freedom, $(\mathbf{Q}, \mathbf{M}) = (Q_{11}, 0, M_1, 0)$ as *order reconstruction* solutions. Moreover, the nodal points of Q_{11} and M_1 in OR solutions are referred to as *domain walls*, since these points correspond to a wall in the xy-plane in the corresponding three-dimensional set-up. A nematic (resp. magnetic) domain wall is a point $y = y^* \in (-1, 1)$ such that $\mathbf{Q}(y^*) = (Q_{11}(y^*), Q_{12}(y^*)) = 0$ (resp. $\mathbf{M}(y^*) = 0$). To see this, we note that for an OR solution, there must exist an interior point, $y^* \in (-1, 1)$ such that $Q_{11}(y^*) = 0$ since $Q_{11}(-1) = 1$ and $Q_{11}(1) = -1$, and $Q_{12}(y) = 0$ for all $y \in [-1, 1]$ by definition; similar remarks apply to the domain wall in $\mathbf{M}$. Furthermore, domain walls in $\mathbf{Q}$ and $\mathbf{M}$ can occur at different points, as we shall see in section 4. OR solutions are special since the domain walls separate polydomains in both $\mathbf{Q}$ and $\mathbf{M}$, i.e., distinctly ordered domains. In fact, recall the parameterisation (2.7) and note that $Q_{12} = M_2 = 0$ implies $\theta = n\pi$ (for some integer n) everywhere; equivalent remarks apply to ϕ. Hence, there is necessarily a domain wall in $\mathbf{Q}$ such that $\theta = 2n\pi$ on one side of the domain wall containing the end point $y = -1$, and $\theta = (2m + 1)\pi$ (for some integers n, m) on the other side of the domain wall containing the end point $y = 1$; analogously, there is a domain wall in $\mathbf{M}$ that separates two polydomains, with $\phi = 2n\pi$ and $\phi = (2m+1)\pi$ for some integers n and m respectively.

We interpret OR solutions as critical points of the following OR energy (which is equivalent to the energy (2.2) with $Q_{12} = M_2 = 0$):

$$\begin{aligned} E(Q_{11}, M_1) \coloneqq \int_{-1}^{1} \Bigg\{ & \frac{l}{2}\left(\frac{\mathrm{d}Q_{11}}{\mathrm{d}y}\right)^2 + \frac{l}{2}\left(\frac{\mathrm{d}M_1}{\mathrm{d}y}\right)^2 + (Q_{11}^2 - 1)^2 \\ & + \frac{1}{4}\left(M_1^2 - 1\right)^2 - cQ_{11}M_1^2 \Bigg\} \, \mathrm{d}y, \end{aligned} \tag{3.1}$$

subject to the boundary conditions

$$\begin{aligned} Q_{11}(-1) &= M_1(-1) = 1, \\ Q_{11}(1) &= M_1(1) = -1, \end{aligned} \tag{3.2}$$

in the admissible space

$$\mathcal{A}' = \left\{ Q_{11}, M_1 \in W^{1,2}(\Omega;\mathbb{R}), Q_{11} \text{ and } M_1 \text{ satisfy the boundary conditions (3.2)} \right\}. \tag{3.3}$$

Hence, OR solutions are classical solutions of the following coupled ordinary differential equations,

$$\begin{aligned} l\frac{\mathrm{d}^2 Q_{11}}{\mathrm{d}y^2} &= 4Q_{11}(Q_{11}^2 - 1) - cM_1^2, \\ l\frac{\mathrm{d}^2 M_1}{\mathrm{d}y^2} &= M_1(M_1^2 - 1) - 2cQ_{11}M_1. \end{aligned} \tag{3.4}$$

In general, we expect multiple OR solutions for fixed values of (l, c) and the optimal OR solution is a minimiser of the energy (3.1) in $\mathcal{A}'$. We give a straightforward existence theorem below, which follows immediately from the direct method in the calculus of variations [13], along with some qualitative properties.

THEOREM 3.1. *(Existence, uniqueness and maximum principle) For all values of (l, c), there exists a minimiser, (Q_{11}^*, M_1^*) of the OR energy (3.1) in $\mathcal{A}'$. This OR minimiser, $(\mathbf{Q}^{OR}, \mathbf{M}^{OR}) = (Q_{11}^*, 0, M_1^*, 0)$, is a solution of the full system (2.5a)-(2.5d), and thus a critical point of the full energy (2.2). Additionally, $(\mathbf{Q}^{OR}, \mathbf{M}^{OR})$ is the unique critical point, and hence, global minimiser of the energy (2.2), for fixed positive c and l large enough, as in Theorem 2.7. Moreover, we have*

$$|Q_{11}(y)| \leq \rho^*, \; M_1^2(y) \leq 1 + 2c\rho^* \quad \forall y \in [-1, 1], \tag{3.5}$$

where ρ^* is given by (2.24).

Proof. Clearly, the admissible space $\mathcal{A}'$ is non-empty as $(Q_{11}, M_1) = (-y, -y) \in \mathcal{A}'$. We observe that (3.1) is lower semicontinuous since it is quadratic and thus, convex in both the gradients of Q_{11} and M_1 [13]. As before, the coupling energy density can be decomposed as follows, for arbitrary $\epsilon > 0$

$$-cQ_{11}M_1^2 \geq -\frac{c}{2}\left(\epsilon Q_{11}^2 + \frac{1}{\epsilon}M_1^4\right).$$

Therefore, the OR energy density is bounded from below as

$$\begin{aligned} &\frac{l}{2}\left(\frac{\mathrm{d}Q_{11}}{\mathrm{d}y}\right)^2 + \frac{l}{2}\left(\frac{\mathrm{d}M_1}{\mathrm{d}y}\right)^2 + (Q_{11}^2 - 1)^2 + \frac{1}{4}\left(M_1^2 - 1\right)^2 - cQ_{11}M_1^2 \\ &\geq \frac{l}{2}\left(\frac{\mathrm{d}Q_{11}}{\mathrm{d}y}\right)^2 + \frac{l}{2}\left(\frac{\mathrm{d}M_1}{\mathrm{d}y}\right)^2 + \left(Q_{11}^2 - \left(1 + \frac{c\epsilon}{4}\right)\right)^2 \\ &\quad + \left(\frac{1}{4} - \frac{c}{2\epsilon}\right)\left(M_1^2 - \frac{\epsilon}{\epsilon - 2c}\right)^2 - \left(\frac{c\epsilon}{2} + \frac{c^2\epsilon^2}{16} + \frac{c}{2(\epsilon - 2c)}\right), \end{aligned}$$

and thus the OR energy (3.1) is coercive for $\epsilon > 2c$. The existence of a minimiser, (Q_{11}^*, M_1^*), of the OR energy (3.1), is an immediate result from [13]. Furthermore,

this minimiser is a (classical) solution of the equations (3.4) subject to the boundary conditions (3.2). It is straightforward to check that the resulting OR solution, $\left(\mathbf{Q}^{OR},\mathbf{M}^{OR}\right)=(Q_{11}^{*},0,M_{1}^{*},0)$ is also a solution of the full system, (2.5a)-(2.5d) and thus, a critical point of the full energy (2.2), in the admissible space (2.4) for all values of (l,c).

Since the full energy (2.2) has a unique critical point for l large enough (see Remark 2.8), we can deduce that $\left(\mathbf{Q}^{OR},\mathbf{M}^{OR}\right)$ is the unique energy minimiser of the full energy (2.2), in the $l\to\infty$ limit.

The bounds (3.5) follow immediately from Theorem 2.5, using the L^{∞} bounds for $|\mathbf{Q}|$ and $|\mathbf{M}|^{2}$ with $Q_{12}=M_{2}=0$. The solution branch $\left(\mathbf{Q}^{OR},\mathbf{M}^{OR}\right)$ exists for all values of (l,c). This completes the proof. ∎

3.1. Homogeneous solutions and asymptotics as $c\to 0$ and $c\to\infty$. By Theorem 2.9, we have that $\left(\mathbf{Q}^{OR},\mathbf{M}^{OR}\right)\to(-y,0,-y,0)$ as $l\to\infty$. The analysis in the $l\to 0$ limit is more involved, which necessitates a computation of the homogeneous solutions (with $\xi=1$) or critical points of the OR bulk potential

$$f^{OR}(Q_{11},M_{1})=(Q_{11}^{2}-1)^{2}+\frac{1}{4}(M_{1}^{2}-1)^{2}-cQ_{11}M_{1}^{2}, \tag{3.6}$$

leading to the following algebraic equations:

$$4Q_{11}(Q_{11}^{2}-1)-cM_{1}^{2}=0, \tag{3.7a}$$

$$M_{1}(M_{1}^{2}-1)-2cQ_{11}M_{1}=0. \tag{3.7b}$$

From (3.7), we have either $M_{1}=0$ and $Q_{11}=\pm 1,0$ for any real-valued c, or $M_{1}^{2}=2cQ_{11}+1$. Following the approach in subsection 2.1, the non-trivial solutions of (3.7) are

$$Q_{11}=\Theta_{1}+\Theta_{2}, \tag{3.8a}$$

$$Q_{11}=\omega_{2}\Theta_{1}+\omega_{3}\Theta_{2}, \tag{3.8b}$$

$$Q_{11}=\omega_{3}\Theta_{1}+\omega_{2}\Theta_{2}, \tag{3.8c}$$

and the corresponding values of M_{1} are

$$M_{1}=\pm\sqrt{2c\left(\Theta_{1}+\Theta_{2}\right)+1}, \tag{3.9a}$$

$$M_{1}=\pm\sqrt{2c\left(\omega_{2}\Theta_{1}+\omega_{3}\Theta_{2}\right)+1}, \tag{3.9b}$$

$$M_{1}=\pm\sqrt{2c\left(\omega_{3}\Theta_{1}+\omega_{2}\Theta_{2}\right)+1}. \tag{3.9c}$$

Again, $\omega_{1}=1$, $\omega_{2}=\frac{-1+\sqrt{3}\mathrm{i}}{2}$ and $\omega_{3}=\frac{-1-\sqrt{3}\mathrm{i}}{2}$ are the cube roots of unity. Therefore, the critical points of the OR bulk potential are ((3.8a),(3.9a)), ((3.8b),(3.9b)) and ((3.8c),(3.9c)). Since $27c^{2}<64\left(1+\frac{c^{2}}{2}\right)^{3}$ for all $c\geq 0$, (3.8a)-(3.8c) are real (by De Moivre's formula) and (3.9a), (3.9c) are real for all positive c, whilst (3.9b) is real for $c\leq\frac{1}{2}$. Therefore, we ignore the pair ((3.8b),(3.9b)) in what follows. It is straightforward to verify from the same plot (see Figure 1) that the pair ((3.8a),(3.9a)) is the global minimiser of the OR bulk potential (3.6), for all values of c.

Next, we compute asymptotic expansions for ((3.8a),(3.9a)), for small and large c. We omit the details as they follow from subsection 2.1. For small c, one can check that

$$Q_{11}\approx 1+\frac{c}{8},\ M_{1}^{2}\approx 1+2c+\frac{c^{2}}{4}.$$

While for large c, we deduce that

$$Q_{11} \approx \left(\frac{\sqrt{2}}{4}\right)^{\frac{1}{3}} c,\ M_1^2 \approx 1 + \sqrt{2}c^2,$$

thus, Q_{11} grows linearly in c and M_1^2 grows quadratically in c, for $c \gg 1$.

Remark 3.2. For $c = 0$, there are nine solution pairs (Q_{11}, M_1), given by (2.22). In the limit $c \to 0$, we expect each of the solution pairs ((3.8a), (3.9a)), ((3.8b), (3.9b)) and ((3.8c), (3.9c)) to reduce to a solution of the uncoupled problem. In fact, we can recover six solution pairs of the uncoupled system with $\sigma \neq 0$. The solutions of the uncoupled system with $\sigma = 0$, exist for all $c > 0$, and are hence, unperturbed by the nemato-magnetic coupling for $c > 0$.

3.2. Convergence analysis in the $l \to 0$ limit. Now, we study the regime of small l (re-scaled elastic constant) which describes macroscopic domains with $D \gg \sqrt{\frac{L}{|A|c^2}}$, for fixed $c > 0$. We define the set of minimisers of the OR bulk potential (3.6):

$$\mathcal{B}^{OR} = \left\{(Q_{11}, M_1) = \left(\rho^*, \sqrt{1 + 2c\rho^*}\right), (Q_{11}, M_1) = \left(\rho^*, -\sqrt{1 + 2c\rho^*}\right)\right\}.$$

As $l \to 0$, we expect that minimisers of the OR energy (3.1) converge to the set $\mathcal{B}^{OR}$ almost everywhere, away from the boundary points $y = \pm 1$. In fact, the boundary conditions, $(Q_{11}(-1), M_1(-1)) = (1, 1)$ and $(Q_{11}(1), M_1(1)) = (-1, -1)$ are not compatible with the solutions in $\mathcal{B}^{OR}$, thus, OR energy minimisers must have boundary layers near $y = \pm 1$ in this limit. We make these heuristics more precise using Γ-convergence results, following the methods in [26].

Consider the rescaled OR energy

(3.10)
$$\frac{1}{\sqrt{l}} E(Q_{11}, M_1) \coloneqq \int_{-1}^{1} \left\{ \frac{\sqrt{1}}{2} \left(\frac{\mathrm{d}Q_{11}}{\mathrm{d}y}\right)^2 + \frac{\sqrt{l}}{2} \left(\frac{\mathrm{d}M_1}{\mathrm{d}y}\right)^2 + \frac{1}{\sqrt{l}} \tilde{f}(Q_{11}, M_1) \right\} \mathrm{d}y$$

where

$$\tilde{f}(Q_{11}, M_1) \coloneqq \left(Q_{11}^2 - 1\right)^2 + \frac{1}{4}\left(M_1^2 - 1\right)^2 - cQ_{11}M_1^2 - \beta(c) \geq 0, \tag{3.11}$$

and the c-dependent constant, $\beta(c)$, is the minimum value of the OR bulk potential. As in [5] and [26], we let $\mathbf{p} = (Q_{11}, M_1)$ and define the following metric d in the $\mathbf{p}$-plane, for any two points $\mathbf{p}_0, \mathbf{p}_1 \in \mathbb{R}^2$:

(3.12)
$$d(\mathbf{p}_0, \mathbf{p}_1) = \inf \left\{ \int_{-1}^{1} \tilde{f}^{1/2}(\mathbf{p}(t)) \left| \frac{\mathrm{d}\mathbf{p}(t)}{\mathrm{d}t} \right| \mathrm{d}t : \mathbf{p}(t) \in C^1\left([-1, 1]; \mathbb{R}^2\right), \mathbf{p}(-1) = \mathbf{p}_0, \mathbf{p}(1) = \mathbf{p}_1 \right\}.$$

Note that this metric is degenerate as $\tilde{f}(\mathbf{p}) = 0$ for $\mathbf{p} = \mathbf{p}^* = \left(\rho^*, \sqrt{1 + 2c\rho^*}\right)$ and $\mathbf{p} = \mathbf{p}^{**} = \left(\rho^*, -\sqrt{1 + 2c\rho^*}\right)$. Despite such degeneracy, the infimum in (3.12) is indeed attained for arbitrary $\mathbf{p}_0$ and $\mathbf{p}_1$ (see [5, Lemma 9] and [26]). Denote $\mathbf{p}_b(1) = (-1, -1)$ and $\mathbf{p}_b(-1) = (1, 1)$. Let $\mathbf{p}_l$ be a minimiser of (3.10) for a fixed $c > 0$. A straightforward application of [26, Proposition 4.1] yields the following theorem.

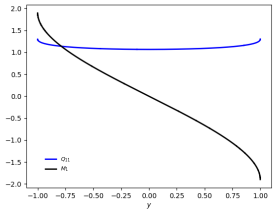

$d(\mathbf{p}^*, \mathbf{p}^{**}) \approx 3.008.$

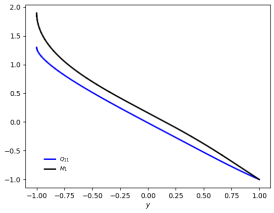

$d(\mathbf{p}^*, \mathbf{p}_b(1)) \approx 3.967.$

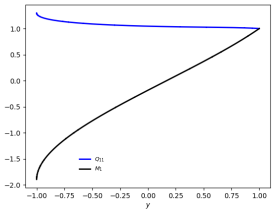

$d(\mathbf{p}^{**}, \mathbf{p}_b(-1)) \approx 2.577.$

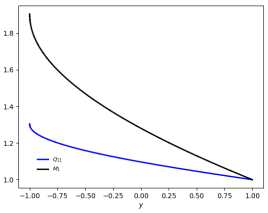

$d(\mathbf{p}^*, \mathbf{p}_b(-1)) \approx 0.455.$

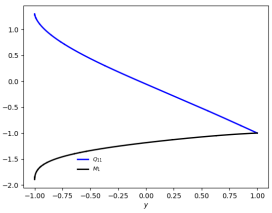

$d(\mathbf{p}^{**}, \mathbf{p}_b(1)) \approx 2.591.$

Fig. 3: The profiles of $\mathbf{p}$ and their corresponding transition costs in (3.14).

THEOREM 3.3. *There exists a subsequence $l_k \to 0$ such that the minimisers $\mathbf{p}_{l_k}$ of (3.10) converge in $L^1([-1,1])$ almost everywhere to a map of the form*

$$\mathbf{p}_0 = \sum_{j=1}^{N} \sum_{i \in \{*,**\}} \mathbf{p}^i \chi_{E_j}$$

where χ is the characteristic function of an interval, $E_j \subset (-1,1)$ such that $\cup_{j=1}^N E_j = (-1,1)$. Moreover, the intervals E_j minimise the following functional

$$J[E_j] := \sum_{j=1}^{N} d(\mathbf{p}^*, \mathbf{p}^{**}) + d\left(\mathbf{p}_0, \mathbf{p}_b(-1)\right) + d\left(\mathbf{p}_0, \mathbf{p}_b(1)\right), \tag{3.13}$$

where the first term describes the number of jumps between $\mathbf{p}^*$ and $\mathbf{p}^{**}$, referred to as interior transition layers that necessarily contain a magnetic domain wall, and the energetic costs of the boundary layers are captured by the second and third terms.

We compute the following transition costs

$$d(\mathbf{p}^*, \mathbf{p}^{**}), d(\mathbf{p}^*, \mathbf{p}_b(1)), d(\mathbf{p}^{**}, \mathbf{p}_b(-1)), d(\mathbf{p}^*, \mathbf{p}_b(-1)), d(\mathbf{p}^{**}, \mathbf{p}_b(1)). \tag{3.14}$$

using the metric (3.12), and we can see from Figure 3 that

$$d(\mathbf{p}^*, \mathbf{p}_b(-1)) < d(\mathbf{p}^{**}, \mathbf{p}_b(-1)) < d(\mathbf{p}^{**}, \mathbf{p}_b(1)) < d(\mathbf{p}^*, \mathbf{p}^{**}) < d(\mathbf{p}^*, \mathbf{p}_b(1)).$$

It is clear that the minimizer of J in (3.13) is $\mathbf{p}^*$, with boundary layers near the edges $y = \pm 1$ and no interior jumps between $\mathbf{p}^*$ and $\mathbf{p}^{**}$.

3.3. Stability of OR solutions. The authors in [18] and [11] consider a similar OR problem with $c = 0$, i.e., in the purely nematic case with $\mathbf{Q} = (Q_{11}, Q_{12})$, in a one-dimensional channel and a two-dimensional square, respectively. In both cases, the

OR solution loses stability as l decreases, or equivalently as the physical channel width D increases, with respect to perturbations that have non-zero Q_{12}. This motivates us to expect a similar instability result in the ferronematic setting with $c > 0$.

THEOREM 3.4. *(Instability of the OR solution) For sufficiently small l and a fixed positive c, the OR energy minimiser, $(\mathbf{Q}^{OR}, \mathbf{M}^{OR})$, is an unstable critical point of the full energy (2.2), in the admissible space (2.4).*

Proof. For the OR solution $(\mathbf{Q}^{OR}, \mathbf{M}^{OR}) = (Q_{11}^*, 0, M_1^*, 0)$, we note that (Q_{11}^*, M_1^*) is a minimiser of the OR energy (3.1). Furthermore, the OR solution depends on l with fixed $c > 0$ and we suppress this explicit dependence for brevity. We compute the second variation of the free energy (2.2) about $\left(\mathbf{Q}^{OR}, \mathbf{M}^{OR}\right)$ with arbitrary perturbations,

$$\begin{aligned}
&\tilde{Q}_{11}(y) = Q_{11}^*(y) + tg(y),\ \tilde{Q}_{12}(y) = th(y),\\
&\tilde{M}_1(y) = M_1^*(y) + tv(y),\ \tilde{M}_2(y) = tw(y).
\end{aligned}$$

Here, $t \in \mathbb{R}$ and $g(y) = h(y) = v(y) = w(y) = 0$ at $y = \pm 1$. The second variation is then given by

$$\begin{aligned}
\delta^2 F[g,h,v,w] &\coloneqq \frac{\mathrm{d}^2}{\mathrm{d}t^2}\bigg|_{t=0} F(\tilde{Q}_{11}, \tilde{Q}_{12}, \tilde{M}_1, \tilde{M}_2)\\
&= \delta^2 E[g,v] + \int_{-1}^{1} \Bigg\{ l\left(\frac{\mathrm{d}h}{\mathrm{d}y}\right)^2 + l\left(\frac{\mathrm{d}w}{\mathrm{d}y}\right)^2 + 4h^2((Q_{11}^*)^2 - 1)\\
&\quad + w^2((M_1^*)^2 - 1) + 2cw^2 Q_{11}^* - 4chwM_1^* \Bigg\} \,\mathrm{d}y\\
&=: \delta^2 E[g,v] + H[h,w],
\end{aligned} \tag{3.15}$$

where $\delta^2 E[g,v]$ is the second variation of the OR energy (3.1) about (Q_{11}^*, M_1^*), and thus necessarily non-negative for all admissible (g,v). To demonstrate the instability of $(\mathbf{Q}^{OR}, \mathbf{M}^{OR})$, we need to construct non-trivial h and w such that $H[h,w] < 0$. To this end, we follow methods in [18] and choose

$$h(y) = \frac{\mathrm{d}Q_{11}^*}{\mathrm{d}y} z(y) =: \tau(y) z(y), \qquad w(y) = \frac{\mathrm{d}M_1^*}{\mathrm{d}y} z(y) =: \zeta(y) z(y), \tag{3.16}$$

where z is a smooth cut-off function with bounded derivatives and $z(y) = 0$ for $|y| > 1 - \eta$, $0 < \eta < \frac{1}{4}$. In particular, we prescribe z so that z and its derivatives can be bounded independently of l. Since h and w vanish at $y = \pm 1$, we have

$$\int_{-1}^{1} \left(h'\right)^2 \,\mathrm{d}y = -\int_{-1}^{1} hh'' \,\mathrm{d}y \quad \text{and} \quad \int_{-1}^{1} \left(w'\right)^2 \,\mathrm{d}y = -\int_{-1}^{1} ww'' \,\mathrm{d}y.$$

Here and hereafter, we take $'$ (resp. $''$) to denote first (resp. second) derivative with respect to y. Furthermore, one can check from (3.4) that

$$\begin{aligned}
&\tau' = \frac{1}{l}\left[4Q_{11}^*\left((Q_{11}^*)^2 - 1\right) - c(M_1^*)^2\right], \quad \tau'' = \frac{1}{l}\left[4\tau\left(3(Q_{11}^*)^2 - 1\right) - 2cM_1^*\zeta\right],\\
&\zeta' = \frac{1}{l}\left[M_1^*\left((M_1^*)^2 - 1\right) - 2cQ_{11}^* M_1^*\right], \quad \zeta'' = \frac{1}{l}\left[\zeta\left(3(M_1^*)^2 - 1\right) - 2cM_1^*\tau - 2cQ_{11}^*\zeta\right].
\end{aligned} \tag{3.17}$$

Now noting $h'' = \tau'' z + 2\tau' z' + \tau z''$, $w'' = \zeta'' z + 2\zeta' z' + \zeta z''$ and substituting (3.16) and (3.17) into $H[h, w]$, we obtain

$$
\begin{aligned}
H[h,w] = &\int_{-1}^{1} \left\{ -8(Q_{11}^*)^2 \tau^2 z^2 + 2\zeta^2 z^2 \left(2cQ_{11}^* - (M_1^*)^2 \right) \right\} \, \mathrm{d}y \\
&+ l \int_{-1}^{1} \left\{ -2zz'\tau\tau' - 2zz'\zeta\zeta' \right\} \, \mathrm{d}y + \int_{-1}^{1} \left\{ -lzz'' \left(\tau^2 + \zeta^2 \right) \right\} \, \mathrm{d}y \\
=: &H_1 + H_2 + H_3.
\end{aligned} \tag{3.18}
$$

The Γ-convergence result in Theorem 3.3 implies that for an interior interval $(a, b) \subset [-1, 1]$, it holds that

$$
\int_a^b |Q_{11}^* - \rho^*| \, \mathrm{d}y \to 0 \quad \text{and} \quad \int_a^b \left| (M_1^*)^2 - 1 - 2c\rho^* \right| \, \mathrm{d}y \to 0 \quad \text{as } l \to 0. \tag{3.19}
$$

Notice that the functions τ and ζ, defined as first derivatives of Q_{11}^* and M_1^* respectively, are bounded in the interior away from $y = \pm 1$. An application of integration by parts implies

$$
\int_{-1}^{1} \left\{ zz'\tau\tau' + zz'\zeta\zeta' \right\} \, \mathrm{d}y = -\frac{1}{2} \int_{-1}^{1} \left\{ \left(z' \right)^2 \left(\tau^2 + \zeta^2 \right) + zz'' \left(\tau^2 + \zeta^2 \right) \right\} \, \mathrm{d}y,
$$

leading to

$$
H_2 \to 0 \quad \text{as } l \to 0.
$$

Moreover, it is straightforward to see that the third integral H_3 in (3.18) vanishes in the $l \to 0$ limit. It remains to estimate the first integral in (3.18). By (3.19), we deduce that

$$
H_1 \to \int_{-1}^{1} \left\{ -8\tau^2 z^2 \left(\rho^* \right)^2 - 2\zeta^2 z^2 \right\} \, \mathrm{d}y < 0 \quad \text{as } l \to 0.
$$

This completes the proof. ∎

4. Numerical results. In this section, we perform numerical experiments to validate our theoretical results and understand the interplay between l and c for the solution landscapes, with fixed $\xi = 1$. For the visualisation, we plot the director $\mathbf{n}$ as rods and the normalised magnetisation vector field $\mathbf{m} = \frac{\mathbf{M}}{|\mathbf{M}|}$ as arrows.

4.1. Solver details. Since the boundary-value problem is nonlinear, we use Newton's method with L^2 linesearch [7, Algorithm 2] as the outer nonlinear solver. The nonlinear solver is deemed to have converged when the Euclidean norm of the residual falls below 10^{-8}, or reduces from its initial value by a factor of 10^{-6}, whichever comes first. For the inner solver, the linearized systems are solved using the sparse LU factorization library MUMPS [1]. The solver described above is implemented in the *Firedrake* [23] library, which relies on PETSc [2] for solving the resulting linear systems. Furthermore, we use the *deflation* technique as described in [15] to compute multiple solutions and bifurcation diagrams. Throughout this section, we partition the whole interval $[-1, 1]$ into 1000 equi-distant subintervals and numerically approximate the solutions using $\mathbb{P}^1$ finite elements (piecewise linear continuous polynomials).

Code availability. For reproducibility and more details of the implementation, we have archived the solver code [27] and the exact version of Firedrake [16] used to

produce the numerical results of this work. An installation of Firedrake with components matching those used in this paper can be obtained by following the instructions at https://www.firedrakeproject.org/download.html with

```
python3 firedrake-install --doi 10.5281/zenodo.4449535
```

Defcon version #aaa4ef should then be installed, as described in https://bitbucket.org/pefarrell/defcon/.

4.2. OR solutions. We have analysed the OR solution branch with $Q_{12} = M_2 = 0$, as $l \to 0$ and as $l \to \infty$. The OR branch is fully characterised by the solutions (Q_{11}, M_1) of the boundary-value problem (3.4). OR solutions are special since they must contain separate domain walls in $\mathbf{Q}$ and $\mathbf{M}$, with the prospect of tailored locations and multiplicities of domain walls by varying l and c.

As $l \to \infty$, recall Theorem 3.1 to deduce that the OR solution branch is approximately given by $\left(\mathbf{Q}^{OR}, \mathbf{M}^{OR}\right) \approx (-y, 0, -y, 0)$, for a fixed c, and that $\left(\mathbf{Q}^{OR}, \mathbf{M}^{OR}\right)$ is also the unique minimiser of both the OR energy (3.1) and the full energy (2.2). In Figure 4, we plot the OR solution of (3.4) for $c = 1$ and $l = 10$. The profile is indeed linear, and we do not numerically obtain any other solutions, supporting the uniqueness result in this regime. The OR solution vanishes at the channel centre $y = 0$, i.e. $Q_{11}(0) = M_1(0) = 0$, and thus both the nematic and magnetic domain walls coincide at $y = 0$. Therefore, the normalised magnetisation vector $\mathbf{m}$ and director $\mathbf{n}$ have a jump discontinuity at $y = 0$, i.e., $\mathbf{m}$ jumps from $\mathbf{m} = (1, 0)$ for $y < 0$ to $\mathbf{m} = (-1, 0)$ for $y > 0$, while $\mathbf{n}$ jumps from $\mathbf{n} = (1, 0)$ (modulo a sign) for $y < 0$ to $\mathbf{n} = (0, 1)$ (modulo a sign) for $y > 0$. The domain walls at $y = 0$ separate two distinct polydomains in $\mathbf{n}$ and $\mathbf{m}$ respectively. We also plot the pointwise L^∞ bound (3.5) as blue solid lines in Figure 4, and as expected, this bound is indeed respected.

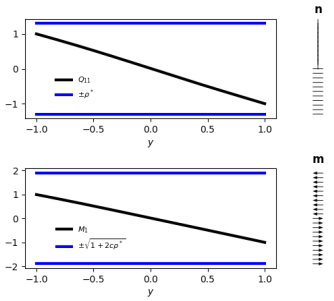

Fig. 4: The only (stable) solution of (3.1) for $c = \xi = 1$, and $l = 10$.

As $l \to 0$ with fixed positive c, we expect to see $Q_{11} \to \rho^*$ uniformly everywhere away from the edges $y = \pm 1$, for the minimiser of the OR energy (3.1), as analysed in section 3. We note that $\rho^*(c)$ defined in (2.24) is an increasing function of c and $\rho^*(0) = 1$, thus $\rho^*(c) > 1$ for all $c > 0$. Similarly, we expect $M_1^2 \to 1 + 2c\rho^*$ away from $y = \pm 1$, for the OR minimiser of (3.1). As discussed in Theorem 3.3, we expect a domain wall in $\mathbf{Q}$ near the edge $y = 1$, within a boundary layer of width $\sqrt{l}$, where Q_{11} jumps from $Q_{11} = \rho^* > 1$ to the boundary value $Q_{11}(1) = -1$. Hence, there necessarily exists a domain wall with $Q_{11} = 0$, within this boundary layer close to $y = 1$. Analogously, there is a boundary layer near the other end point $y = -1$, within which Q_{11} jumps from $Q_{11}(-1) = 1$ to $Q_{11} = \rho^*$. However, this boundary layer does not contain a domain wall with $Q_{11} = 0$. Moreover, we expect that there are at least

two OR minimisers of the OR energy (3.1) for l small enough, with opposite signs of M_1 in the interior domain, away from $y = \pm 1$. Each of these minimisers must contain at least one magnetic domain wall: near $y = 1$ if $M_1 > 0$ in the interior, or near $y = -1$ if $M_1 < 0$ in the interior respectively. Of course, all OR solutions are unstable critical points of the full energy (2.2) in the $l \to 0$ limit, as proven in Theorem 3.4. In what follows, a transition layer refers to a thin interval within which M_1 jumps between $-\sqrt{1+2c\rho^*}$ and $\sqrt{1+2c\rho^*}$ and each of these transition layers necessarily contains a magnetic domain wall with $M_1 = M_2 = 0$. Furthermore, we expect the OR energy (3.1) to have multiple critical points, with multiple interior transition layers and domain walls in $\mathbf{Q}$ and $\mathbf{M}$ for l small enough, although we have no analytical results for non-minimising critical points of (3.1). We now numerically corroborate these theoretical conjectures with $l = 0.01$ and $\xi = 1$.

In Figure 5, we present four example solutions with $c = 1$. In fact, they are all unstable critical points of the full energy (2.2) whilst being stable critical points of the OR energy (3.1) (in the sense that the Hessian of second variation of the OR energy about these critical points has positive eigenvalues). As expected, these solution profiles, (Q_{11}, M_1), have boundary layers near the end points. Furthermore, interior transition layers in M_1 (near the centre $y = 0$) are observed in Solutions 3 and 4. The L^∞ bounds (3.5) (blue solid line) for $|Q_{11}|$ and $|M_1|$ are also satisfied.

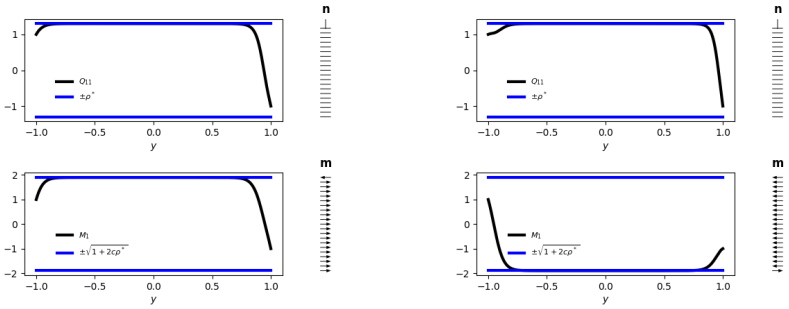

(Solution 1) (Solution 2)

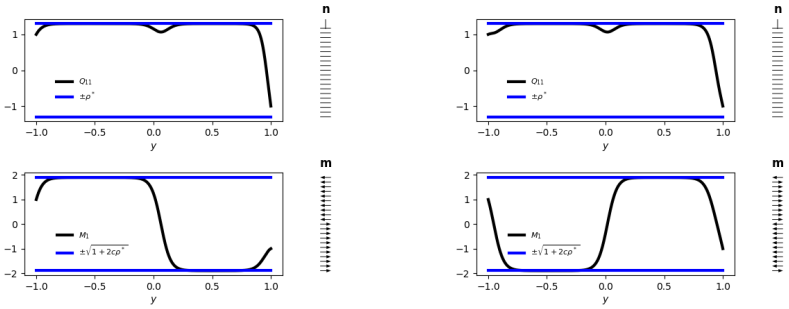

(Solution 3) (Solution 4)

Fig. 5: Four OR solution profiles with $c = \xi = 1$ and $l = 0.01$. Solution 1 is the OR energy minimiser. (3.1).

In Figure 6, we plot the stable stationary profiles of the OR energy (3.1) for a larger value $c = 5$, which are unstable critical points of the full energy (2.2). Indeed,

each of the solutions in Figure 6 has one unstable eigendirection, in the context of the full energy (2.2). The two profiles in Figure 6, have boundary layers near $y = \pm 1$, and essentially differ in the sign of M_1 in the interior; Q_{11} only vanishes near $y = 1$ as predicted by the Γ-convergence analysis, so that we have a nematic domain wall near $y = 1$. On the other hand, M_1 can vanish either near $y = -1$ or near $y = 1$, so that the corresponding magnetic domain wall can occur near either boundary. Additionally, there are other solutions with interior transition layers for M_1, see two examples in Figure 7 where single and multiple interior transition layers in M_1 are observed. They are also stable critical points of the OR energy (3.1), and unstable critical points of the full energy (2.2). The transition layers in M_1 necessarily contain a magnetic domain wall with $M_1 = 0$, and these interior magnetic domain walls are not accompanied by associated nematic domain walls. Moreover, solutions with interior transition layers have higher OR energy (3.1) than solutions without interior transition layers in Figure 6, since each transition layer has an energetic cost of $d(p^*, p^{**})$ as explained in Theorem 3.3.

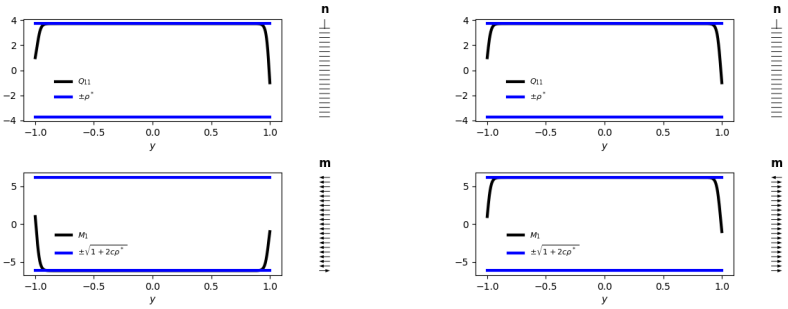

Fig. 6: Two stable OR critical points of (3.1), for $c = 5$, $\xi = 1$ and $l = 0.01$. The right profile has lower OR energy than the left profile and the solutions in Figure 7.

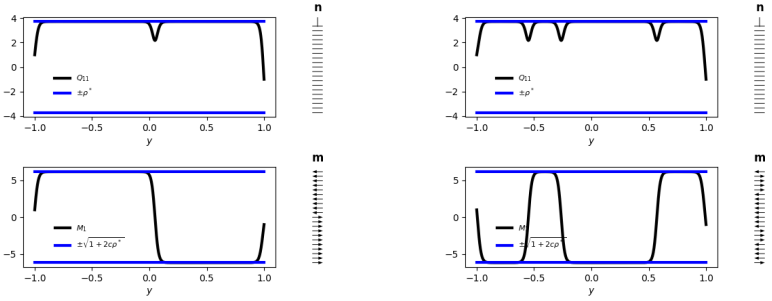

Fig. 7: Two stable OR solutions with single (left) and multiple (right) interior transition layers for $c = 5$, $\xi = 1$ and $l = 0.01$. The left profile has lower OR energy than the right profile.

These numerical experiments illustrate, amongst other aspects, that we can manipulate the location and multiplicity of nematic and magnetic domain walls in the

OR solutions by varying l, e.g., the domain walls in the OR energy minimisers migrate from the channel centre to the channel boundaries at $y = \pm 1$, as l decreases.

4.3. Solutions of the full problem. In this subsection, we focus on the full problem (2.5a)-(2.5d) with four degrees of freedom, $(Q_{11}, Q_{12}, M_1, M_2)$ as opposed to OR solutions with only two degrees of freedom. We only consider the case of small $l_1 = l_2 = l = 0.01$ with $\xi = 1$, since the OR solution branch is the unique solution of the full problem as $l \to \infty$ and OR solutions have been discussed at length in the preceding subsection.

In Figure 8, we take $c = 1$ and present four examples of stable stationary profiles $(Q_{11}, Q_{12}, M_1, M_2)$. One can compare the L^∞ bound (2.23) with the computed values of $|\mathbf{Q}| = \sqrt{Q_{11}^2 + Q_{12}^2}$ and $|\mathbf{M}| = \sqrt{M_1^2 + M_2^2}$ in the figure, illustrating that the pointwise maximum principle in Theorem 2.5 is verified. There are no interior domain walls with $|\mathbf{Q}| = |\mathbf{M}| = 0$, for small l, as discussed in subsection 2.3. Furthermore, Solutions 1, 2 and 3 in Figure 8 only have boundary layers, with constant $|\mathbf{Q}|, |\mathbf{M}|$-profiles in the domain interior, whereas Solution 4 has interior non-zero local minima in $|\mathbf{Q}|$ and $|\mathbf{M}|$. Solutions 1 and 2 are the energy minimisers while the remaining two profiles are non-minimising stable critical points of the full energy (2.2). Note that the two energy minimisers differ in their $\mathbf{m}$-patterns (more precisely, the sign of M_2). Moreover, we compute the values of θ, ϕ defined to be

$$\theta = \arctan\left(\frac{Q_{12}}{Q_{11}}\right), \ \phi = \arctan\left(\frac{M_2}{M_1}\right) \tag{4.1}$$

for each numerical solution profile $(Q_{11}, Q_{12}, M_1, M_2)$, so to verify the relation (2.40). It can be seen that $|\mathbf{Q}| \to \rho^*, |\mathbf{M}| \to 1 + 2c\rho^*$ for the energy minimiser (Solution 1), whereas $(2\phi - \theta)$ tends to an even multiple of π almost everywhere, except near the end point $y = 1$. We do not attempt to explain the interior jumps in the plots of $(2\phi - \theta)$ for Solutions 3 and 4, except that these jumps will have a distinct optical signature in physical experiments. Furthermore, the separate plots of θ and ϕ demonstrate linear behaviour except around the local minima and boundary layers, consistent with the limiting Laplace equations (2.40) for ϕ and θ, in the $l \to 0$ limit.

Now, we repeat the simulations for $c = 5$. Two stable stationary profiles are illustrated in Figure 9. We see that $|\mathbf{Q}| \to \rho*$ and $|\mathbf{M}|^2 \to 1 + 2c\rho^*$ almost everywhere, as expected. Here, Solution 2 has lower energy than Solution 1, since Solution 1 has more local minima in $|\mathbf{Q}|$ and $|\mathbf{M}|$ than Solution 2. Further, $(2\phi - \theta)$ is an even multiple of π almost everywhere, with the jumps being associated with the local minima in $|\mathbf{Q}|$ and $|\mathbf{M}|$, thus verifying the constraint (2.40b). Additionally, we plot ϕ and θ in Figure 9, and observe almost linear profiles of θ and ϕ, except around the local minima and the boundary layers. To summarise, the numerical experiments and the heuristics in Section 2.3 suggest that there are at least two energy minimisers, characterised by $(\rho_1, \sigma_1, \theta_1, \phi_1)$ and $(\rho_2, \sigma_2, \theta_2, \phi_2)$ of (2.2) in the $l \to 0$ limit, such that $\rho_1, \rho_2 \to \rho^*$, $\sigma_{1,2}^2 \to 1 + 2c\rho^*$ almost everywhere away from $y = \pm 1$, $\theta_2 = -\theta_1$, $\phi_2 = -\phi_1$, with no domain walls and $2\phi_{1,2} - \theta_{1,2}$ an even multiple of π except near $y = 1$. The two energy minimisers differ in the sense of rotation, in $\mathbf{n}$ and $\mathbf{m}$, between $y = -1$ and $y = 1$.

4.4. Bifurcation diagram with continuing l. We vary $l_1 = l_2 = l \in [0.2, 3.0]$ with step size 0.01 and $c = 1$ in Figure 10. There is only one stable OR solution for $l \in [1.25, 3.0]$, being the energy minimiser of the full energy (2.2). For $l \approx 1.25$, there is a pitchfork bifurcation consisting of two stable branches and one unstable OR branch (see Figure 11 for an illustration of these three solutions at $l = 1$). In fact,

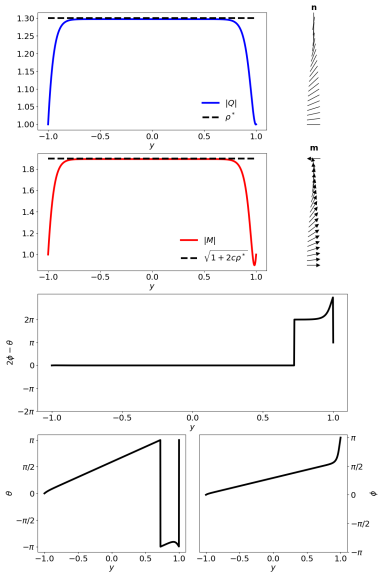

(Solution 1; stable)

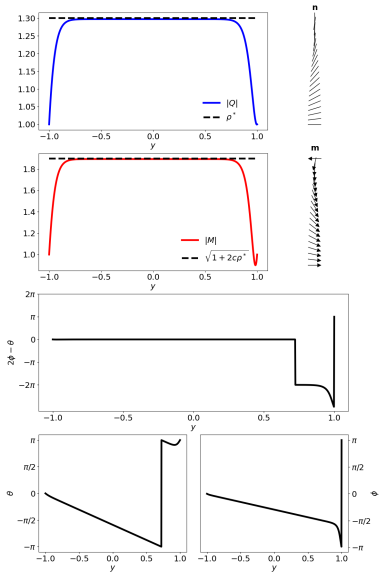

(Solution 2; stable)

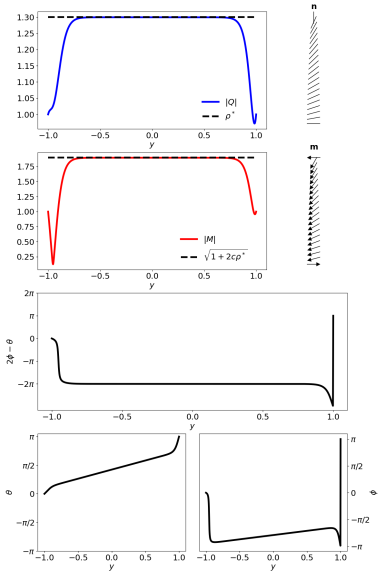

(Solution 3; stable)

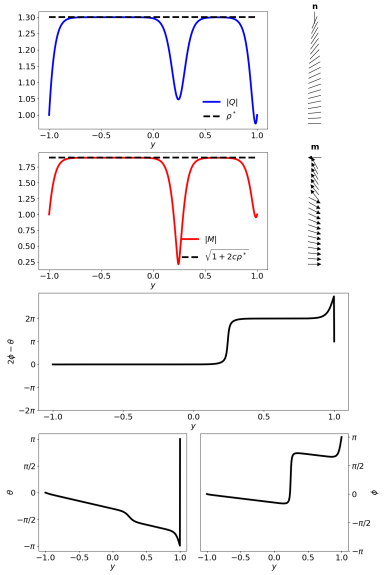

(Solution 4; stable)

Fig. 8: Four stable stationary profiles, $(Q_{11}, Q_{12}, M_1, M_2)$, of (2.2) with $l = 0.01$ and $c = \xi = 1$, along with plots of $(2\phi - \theta)$, θ, and ϕ to verify the relation (2.40). Solutions 1 and 2 have the lowest full energy value (2.2).

the two stable solutions (Solutions 1 and 3 in Figure 11) differ by the sign of Q_{12} and M_2, i.e., for every solution branch, $(Q_{11}, Q_{12}, M_1, M_2)$, there exists another solution branch with $(Q_{11}, -Q_{12}, M_1, -M_2)$. The stable solution branches correspond to a smooth rotation in $\mathbf{n}$, between the two end points $y = \pm 1$ and are actually the global

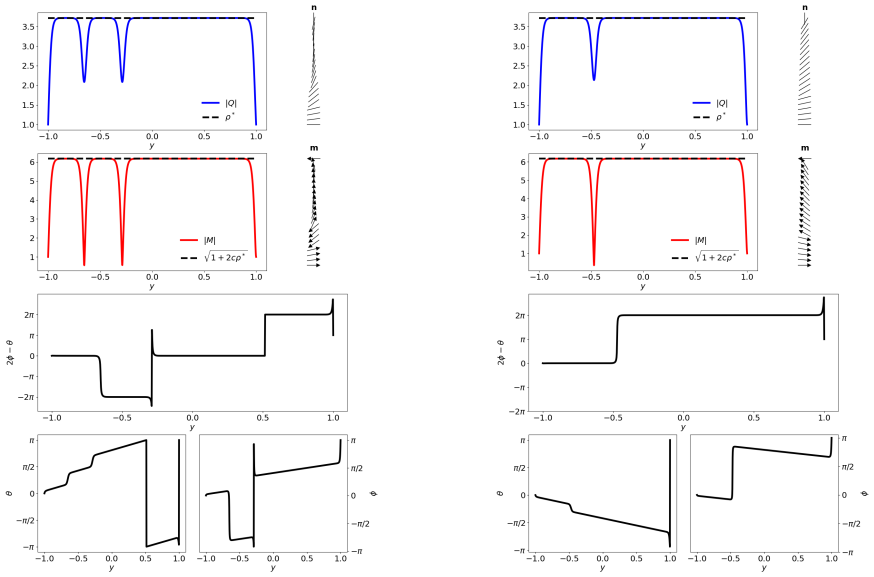

(Solution 1; stable) (Solution 2; stable)

Fig. 9: Two examples of stable stationary profiles $(Q_{11}, Q_{12}, M_1, M_2)$ of the full energy (2.2) with $l = 0.01$, $c = 5$ and $\xi = 1$. Solution 2 has lower energy than Solution 1.

energy minimisers for $l \leq 1.25$.

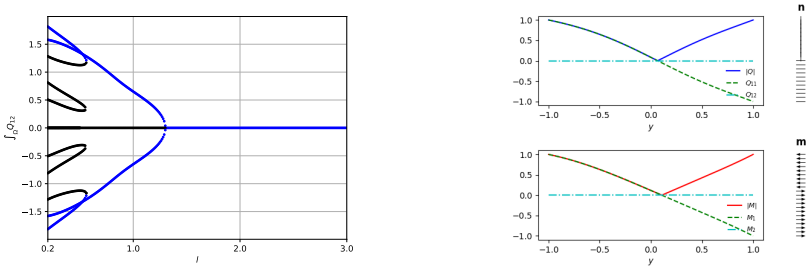

Fig. 10: Left: the bifurcation diagram of continuing $l_1 = l_2 = l \in [0.2, 3.0]$ with fixed $c = \xi = 1$; here, black represents unstable solutions while blue indicates stable solutions. Right: the stable solution for $l = 2$.

As l becomes smaller, more (stable or unstable) solutions are found. More specifically, there are four disconnected bifurcations appearing around $l = 0.55$, giving two further stable solutions, which are also local energy minimisers (see Solutions 1 and 8 in Figure 12 for an illustration) for $l \in [0.2, 0.55]$. Again, they only differ by the sign of Q_{12} and M_2. In Figure 12, we plot eight newly found solution profiles, along with their stabilities. The stable solutions typically correspond to a smooth **n**-profiles with minimal rotation (minimal topological degree consistent with the boundary conditions) , while the stable normalised magnetisation profiles **m** are also smooth, except

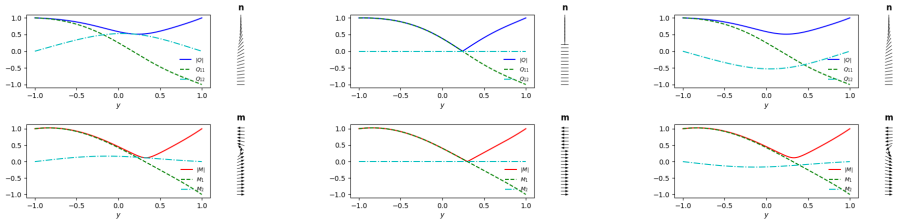

(Solution 1; stable) (Solution 2; unstable) (Solution 3; stable)

Fig. 11: Three solutions for $l = 1$ in Figure 10. Solutions 1 and 3 are global energy minimisers.

for a thin interval of large rotation in $\mathbf{m}$ localised near the end points $y = \pm 1$. Meanwhile, it can be seen that the unstable solution pairs, i.e., Solutions 2 & 7, Solutions 3 & 6 and Solutions 4 & 5 also differ by the sign of Q_{12} and M_2. Interestingly, all profiles with interior jumps in $\mathbf{n}$ and $\mathbf{m}$ are unstable.

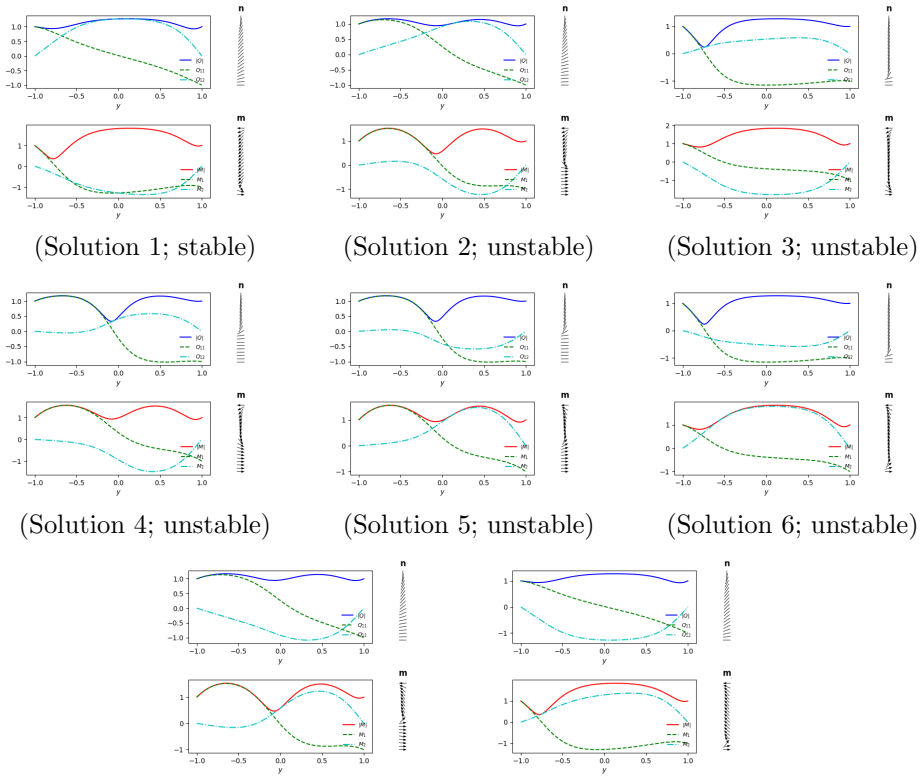

(Solution 1; stable) (Solution 2; unstable) (Solution 3; unstable)

(Solution 4; unstable) (Solution 5; unstable) (Solution 6; unstable)

(Solution 7; unstable) (Solution 8; stable)

Fig. 12: Eight new solutions for $l = 0.2$ in Figure 10. Solutions 1 and 8 are global energy minimisers.

We next investigate the loss of stability of the OR solution branch for a larger value of c, i.e., we numerically compute a bifurcation diagram in Figure 13, for the solutions of (2.5a)-(2.5d), by continuing $l \in [3, 5]$ with a step size of 0.015, and fixed $c = 5$. One stable OR solution is shown in Figure 13 and it loses stability at the pitchfork bifurcation point $l \approx 4.46$, leading to two new stable branches (see illustrations in Figure 14 for $l = 4.43$). We observe that they only differ in the signs of Q_{12} and M_2 and in fact are energy minimisers for $l \leq 4.34$. Thus, the qualitative features of the bifurcation diagram are unchanged by increasing c but the OR solution branch loses stability for $l < l^*(c)$, where $l^*(c)$ is an increasing function of c. Hence, as c increases, OR solutions are increasingly difficult to find owing to their shrinking window of stability.

Remark 4.1. One may wonder about the appearance of the two folds in the bifurcation diagram depicted in Figure 13. They do not represent the same solution at the intersection points. Instead, they are just overlapping points in this plot of $\int_\Omega Q_{12}$ against l. Choosing a different functional may yield a bifurcation diagram without these intersection points.

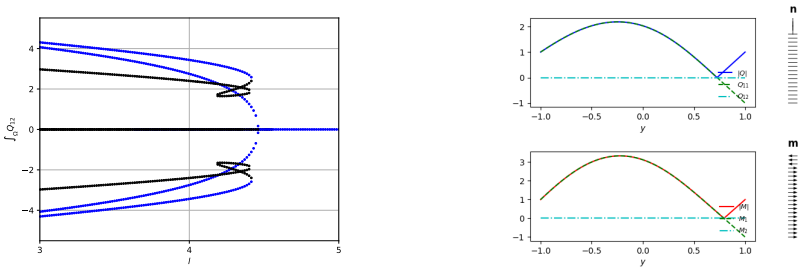

Fig. 13: Left: the bifurcation diagram with fixed $c = 5$ and $\xi = 1$; here, black labels unstable solutions while blue labels stable solutions. Right: one stable OR solution for $l = 4.45$.

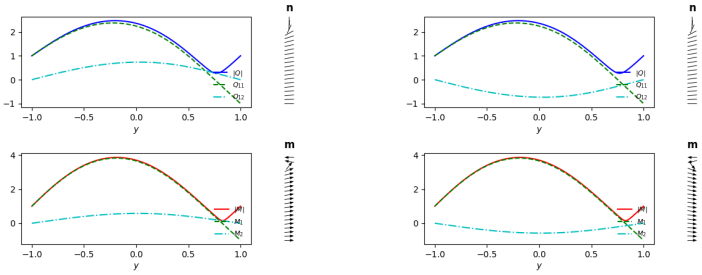

Fig. 14: Two new stable solutions at $l = 4.43$ in Figure 13.

5. Conclusions. We study confined systems with nematic and magnetic orders inside a channel geometry with Dirichlet boundary conditions. Specifically, we model the stable equilibria as minimisers of an appropriately defined energy on an interval

$[-D, D]$, with three contributions: a nematic energy, a magnetic energy and a nemato-magnetic coupling energy. We are interested in two parameters: the scaled elastic parameter l that is proportional to the ratio of a material-dependent length scale (typically the magnetic or nematic correlation length) and D, and the coupling parameter c. We rigorously show that c effectively scales the nematic correlation length ξ_n as $\frac{1}{c}\xi_n$ for large c and thus we have the unique OR solution for $D \ll c_1 \frac{\xi_n}{\sqrt{c_0^2+c^2}}$. The OR solution has nematic and magnetic domain walls; these domain walls can be labelled as nematic or magnetic defects with distinct optical signatures. As D increases for fixed c (or c increases for fixed D), there can be multiple OR solutions, all of which are unstable, and the stable solutions do not have domain walls or poly-domains for large D. There are multiple stable solutions for large D, characterised by the rotation profiles of $\mathbf{n}$ and $\mathbf{m}$ between the channel walls. Our choice of boundary conditions necessarily lead to boundary layers, which will have a distinct optical signature if implemented. We have further provided analytic characterisations of the limiting profiles for small D (in terms of the OR solution) and large D (in terms of limiting maps) accompanied by extensive numerical studies, which beautifully illustrate the co-existence of interior transition layers, boundary layers and multiple stable and unstable critical points as either D or c increases. This work gives informative insight into the complex interplay between geometry, material properties, temperature (captured by l), nemato-magnetic coupling and boundary conditions in the solution landscapes and observable defects.

The methods presented in this work can be modified to include the effects of topological degrees of imposed boundary conditions, weak anchoring and different types of nemato-magnetic coupling, which could enhance the stability of OR solutions, as opposed to suppressing the stability of OR solutions as with our example of nemato-magnetic coupling valid for dilute ferronematics.